nature communications

Article

https://doi.org/10.1038/s41467-026-74843-x

Reprogramming the lipid peroxidation product 4-ONE as a chemoselective cleavable crosslinker

Received: 4 November 2025

Accepted: 16 June 2026

Published online: 25 June 2026

Check for updates

Zachary E. Paikin[1], John M. Talbott[1], Anthony M. Ciancone[2], Samrat Kundu[1], Sukhendu Manna[1], Bao Quang Gia Le[1], Hitendra Negi[3], Kylie J. Walters[3], Francis J. O'Reilly[2,4] & Monika Raj[1]

Lipid peroxidation products modify proteins during oxidative stress, but the residue-pair connectivity and structural consequences of these reactions remain difficult to define. Here, we redefine the lipid peroxidation product 4-oxo-2-nonenal (4-ONE) from a damaging electrophile into a chemoselective Cys-Lys covalent crosslinker. Through a chemoselective, two-step pathway, Michael addition to cysteine activates a latent aldehyde that cyclizes with lysine to form a stable pyrrole linkage under physiological conditions. We show that this chemistry supports late-stage peptide functionalization, macrocyclization and stapling, selective protein modification, and proteome-wide mapping of 4-ONE-reactive lysine and cysteine residues. Additionally, late-stage oxidation converts this pyrrole linkage into an MS-cleavable sulfoxide for site-resolved identification of linked residues through diagnostic link-site-containing fragments, a workflow we name COSMIc (Crosslink Oxidation to Sulfoxide for Mass-Cleavable Interactomics). COSMIc enables detection of structurally informative crosslinks in the human 26S proteasome, where peroxide-induced sulfoxide formation markedly improves fragment assignment and residue-pair confidence. Together, these findings repurpose 4-ONE from a toxic electrophile into a compact, metabolite-derived Cys-Lys crosslinker for covalent mapping and structural proteomics.

Covalent crosslinking is one of nature's most powerful strategies for building and stabilizing molecular architecture. Enzymes, such as transglutaminases, generate selective covalent bonds that reinforce biomolecular assemblies (Fig. 1A)[1,2]; at the same time, biology also exploits a less appreciated strategy: under damage or stress, reactive small molecules can be unmasked to rapidly crosslink proteins, reshape proteomes, and generate protective materials[3–16]. Lipid peroxidation converts membrane lipids into reactive electrophiles that covalently modify proteins during oxidative stress. Among these products, 4-oxo-2-nonenal (4-ONE) is particularly reactive, forming stable adducts with nucleophilic residues and altering proteins involved in proteostasis, metabolism, and redox regulation. These reactions, although widely implicated in oxidative stress, aging, and disease, are more typically dismissed as diffuse chemical damage, and, as a result, the covalent architectures they generate remain poorly defined and challenging to resolve using conventional crosslinking-MS workflows[17–27].

[1]Department of Chemistry, Emory University, Atlanta, GA, USA. [2]Structural System Biology Section, Center for Structural Biology, National Cancer Institute (NCI), National Institutes of Health, Frederick, MD, USA. [3]Protein Processing Section, Center for Structural Biology, National Cancer Institute (NCI), National Institutes of Health, Frederick, MD, USA. [4]Department of Structural Biology, Center of Excellence for Data Driven Discovery, St Jude Children's Research Hospital, Memphis, TN, USA. e-mail: monika.raj@emory.edu

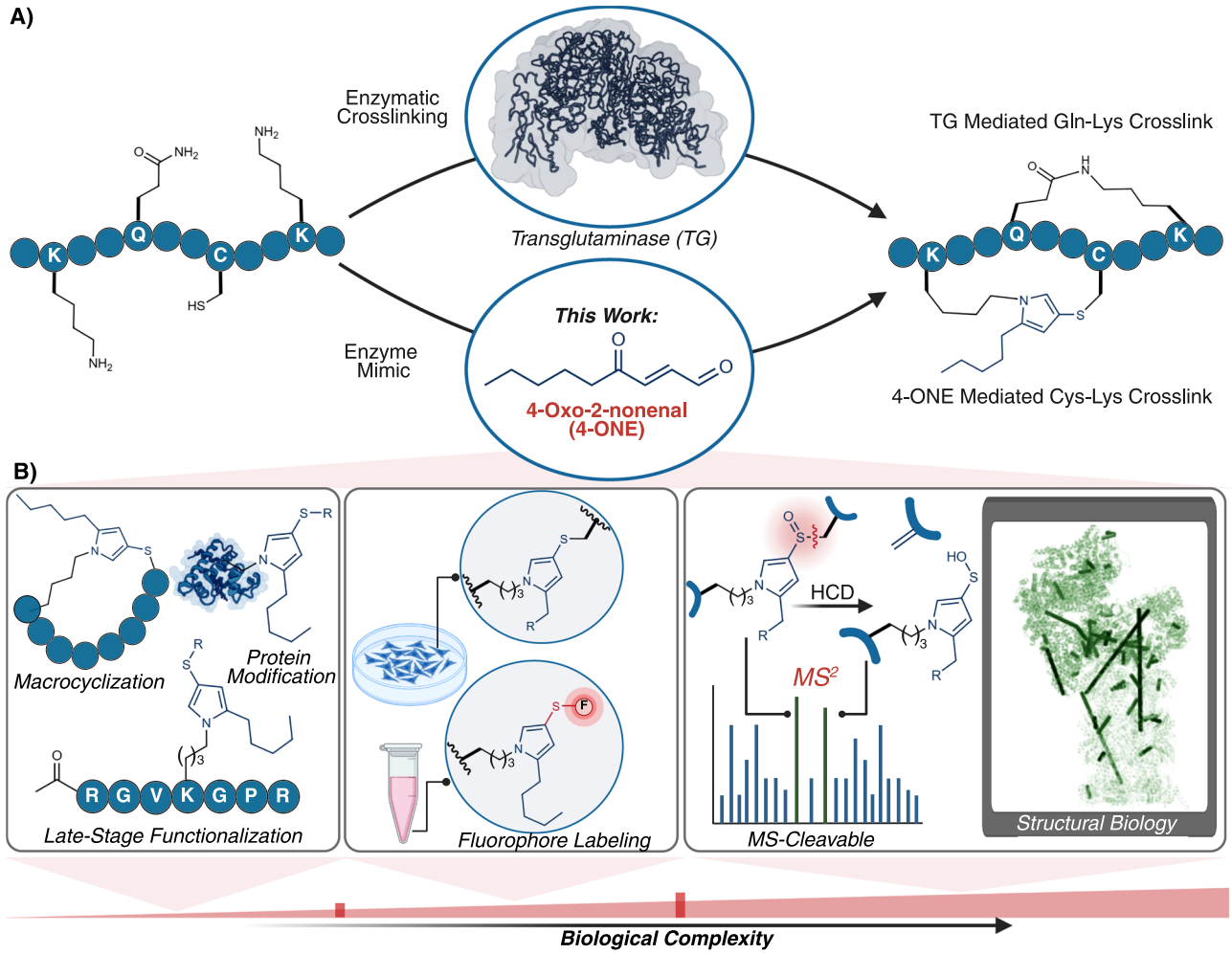

Fig. 1 | 4-ONE as a covalent chemical crosslinker for selective Cys-Lys crosslinking at various levels of complexity. A Transglutaminase (TG) catalyzes crosslinking between glutamine (Gln) and lysine (Lys), whereas 4-ONE generates a Cys-Lys pyrrole linkage. **B** Utilization of 4-ONE as a covalent chemical crosslinker across levels of complexity, from late-stage functionalization (LSF) of peptides and cyclization/stapling to proteome-wide crosslinking in live cells and structural mapping in native protein assemblies. Late-stage oxidation of the 4-ONE-derived pyrrole crosslinks to sulfoxide renders the linkage MS-cleavable through diagnostic sulfenic acid and dehydroalanine fragments, enabling site-resolved identification of linked residues and structurally informative crosslinks without the pre-installation of a synthetic, MS-cleavable moiety. *Created in BioRender. Lab, R. (2026)* https://BioRender.com/bjzaexi.

Here, we repurpose the lipid peroxidation product 4-ONE, a toxic by-product of oxidative stress, into a chemoselective, covalent crosslinker. We show that 4-ONE operates through a defined, two-step mechanism, in which Michael addition by cysteine activates a latent aldehyde that cyclizes with lysine to form a stable Cys-Lys pyrrole crosslink under physiological conditions (Fig. 1A-B). This reaction is highly chemoselective, requires the cooperative participation of both residues, and generates well-defined heterocyclic linkages.

We further demonstrate that late-stage oxidation converts the Cys-Lys pyrrole into an MS-cleavable sulfoxide, yielding orthogonal MS/MS signatures: sulfenic acid on lysine and dehydroalanine on cysteine, that arise only after bona fide crosslink formation (Fig. 1B). We dub this strategy COSMIc (Crosslink Oxidation to Sulfoxide for Mass-Cleavable Interactomics): a platform for site-resolved mapping of metabolite-driven crosslinks in native environments. We apply 4-ONE crosslinking across levels of complexity, from peptide functionalization, macrocyclization, and stapling, to selective protein labeling, proteome-wide profiling, and structurally informative crosslinking in the human 26S proteasome. Together, these findings reposition 4-ONE as a compact, metabolite-derived, Cys–Lys crosslinker for covalent mapping and structural proteomics.

Results and discussion

4-ONE as a Cys-Lys covalent crosslinker

We began our studies using a model peptide, Ac-GKFV **1a**, and subjected it to five equivalents of 4-ONE (see Supplementary Fig. 1 for synthesis) under physiological conditions (pH 7.4) at 37 °C for 24 h (Fig. 2A, Supplementary Fig. 1). Contrary to our expectations and previous reports, we did not detect any stable adduct formation with lysine under the conditions of our HPLC-MS analysis[28,29].

Next, we modified our experiment by adding butanethiol to peptide **1a** in the presence of 4-ONE. Remarkably, more than 95% conversion of lysine to the pyrrole product **2a** was achieved within 5 h at 37 °C, using 3 equiv. each of 4-ONE and butanethiol (Fig. 2A, Supplementary Fig. 1). We hypothesized that this transformation would generate two regioisomeric pyrrole products, arising from thiol addition at the 1,4-position relative to either the aldehyde group of 4-ONE to give regioisomer 1 or the ketone group to give regioisomer 2 (Fig. 2B and Supplementary Fig. 2). To test this hypothesis, we scaled up the reaction using butylphenylamine and ethanethiol as model substrates. The two 4-ONE-derived pyrrole regioisomers were obtained in a 1:1 ratio, as determined by ^{1}H NMR analysis of the crude reaction mixture. The regioisomers were then separated by column chromatography and independently characterized by ^{1}H, ^{13}C, COSY, HSQC, and HMBC

https://doi.org/10.1038/s41467-026-74843-x

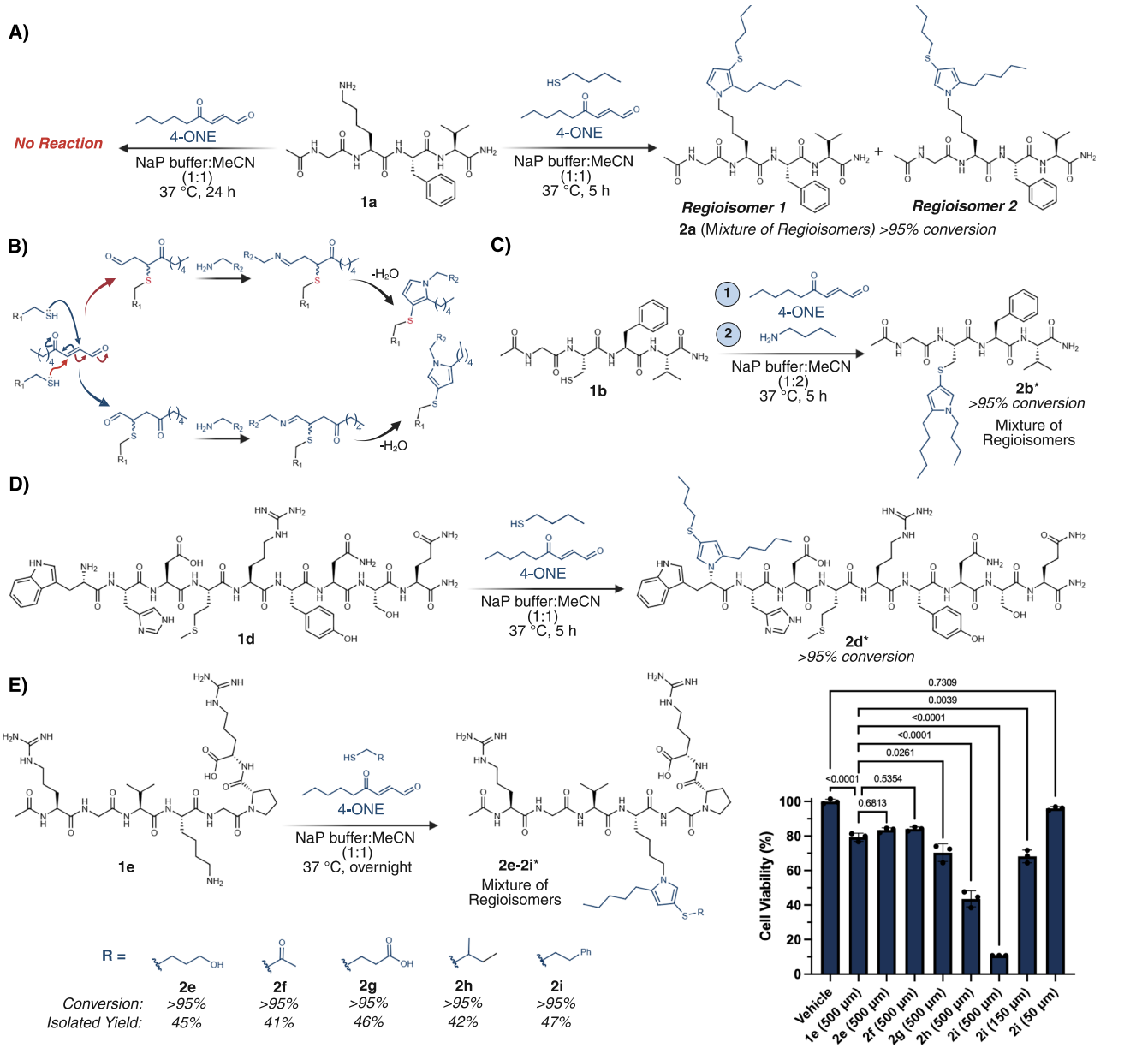

Fig. 2 | Development of 4-ONE-mediated Cys–Lys crosslinking. A Reaction of Lys-containing peptide Ac-GKFV **1a** with 4-ONE (5 equiv.) under physiological conditions produced no Lys adduct. In contrast, the presence of both butanethiol and 4-ONE (3 equiv. each) resulted in efficient (>95%) conversion of **1a** to the pyrrole crosslink regioisomers **2a**. **B** Proposed mechanism of 4-ONE pyrrole formation: sequential Cys Michael addition followed by Schiff base formation, cyclization and oxidation to generate two pyrrole regioisomers depending on the site of initial Cys addition. **C** Cys-containing peptide Ac-GCFV **1b** reacts with 4-ONE (3 equiv.) via initial Michael addition to yield intermediate **2b′**, followed by Schiff-base formation with butylamine, subsequent intramolecular cyclization and oxidation to furnish pyrrole product **2b**. **D** Chemoselectivity analysis using peptide H_2N-WHDMRYNSQ **1d** containing multiple reactive residues demonstrated exclusive modification at the N-terminal amine only in the presence of thiol and 4-ONE (5 equiv. each), affording pyrrole product **2d** in >95% conversion with no detectable side products. **E** Late-stage functionalization of cytotoxic peptide Ac-RGVKGPR **1e** with diverse substituted thiols and 4-ONE (5 equiv. each) generated a library of pyrrole-modified peptides (**2e**-**2i**). Flow cytometry analysis of MCF-7 cells treated with these peptides revealed variable cytotoxic profiles, with derivative **2i** exhibiting the greatest enhancement in cell death relative to the parent peptide **1e** ($p < 0.0001$ for 500 μM dosing condition). Error bars represent mean ± standard deviation ($n = 3$ biological replicates). Statistical analysis was determined by one-way ANOVA; p-values are displayed in the figure. Source data are provided as a Source Data file. *Representation depicts one of the possible regioisomers generated by the 4-ONE cross-coupling. *Created in BioRender. Lab, R. (2026)* https://BioRender.com/qas0ih7.

NMR spectroscopy. These data confirmed the formation of two distinct pyrrole connectivities, consistent with thiol addition at the two electrophilic positions of 4-ONE (Supplementary Fig. 2). To determine whether this 1:1 regioisomeric ratio was consistent across different substrates, we performed a second scaled-up reaction using butylphenylamine and methyl 3-mercaptopropionate as model substrates. In this case, the reaction produced the two regioisomers in a 2:1 ratio, as determined by ^{1}H NMR analysis of the crude mixture. After chromatographic separation, structural characterization using ^{1}H, ^{13}C, COSY, HSQC, and HMBC NMR spectroscopy confirmed that regioisomer 1, arising from thiol addition at the 1,4-position relative to the aldehyde group, was the major product (Supplementary Fig. 2).

Since the reaction is multi-step, including a Michael addition to cysteine (Cys), followed by Schiff base formation with the amine,

cyclization, and subsequent oxidation to form the heterocyclic pyrrole ring (Fig. 2B), we sought to optimize and capture intermediates by analyzing the reaction with the Cys-containing peptide Ac-GCFV **1b** (Fig. 2C, Supplementary Fig. 3). We added 4-ONE and analyzed the reaction at regular intervals. Interestingly, we observed the formation of a mono Michael addition product **2b′** within 2 h under physiological conditions when the reaction was carried out with Cys. No other intermediates were detected upon addition of butylamine to the Michael addition product **2b′**. This suggests that once the Michael adduct forms with Cys, it spontaneously reacts with butylamine, converting to a stable pyrrole product **2b** with over 95% conversion (Fig. 2C, Supplementary Fig. 3). In an attempt to form crosslinks between histidine (His) and Lys, we replaced Cys with His and tested the peptide Ac-GHFV **1c** for the initial Michael addition reaction with 4-ONE (Supplementary Fig. 3). However, no Michael adduct was formed with the Ac-GHFV peptide. Similarly, no product or intermediate was observed when lysine was used alone with 4-ONE without thiol as shown with peptide **1a** (Fig. 2A). These findings strongly suggest that for Lys to react with 4-ONE, a prior Michael addition with Cys is required. This is in contrast to prior studies, which reported the formation of various products when Lys reacts with 4-ONE, as no such reaction was observed in our studies when Lys was reacted alone[28,29].

These observations suggested that 4-ONE-mediated pyrrole formation is not simply a consequence of electrophile reactivity but instead depends on a defined cooperative relationship between thiol and amine partners, prompting us to examine how this mechanism behaves in the presence of competing nucleophilic residues.

Chemoselectivity of 4-ONE-mediated crosslinking

Having established that pyrrole formation proceeds through cysteine-first activation of 4-ONE, we next asked whether this reactivity would remain selective in the presence of other nucleophilic amino acids commonly found in peptides and proteins. To test this and further assess the specificity of lysine (Lys) in forming the pyrrole-crosslink adduct with thiols, we subjected the peptide H_2N-WHDMRYNSQ **1d**, containing diverse reactive amino acids (Trp, His, Asp, Met, Arg, Tyr, Asn, Ser, Gln, and the N-terminus), to the optimized reaction conditions with 4-ONE, both with and without butanethiol (Fig. 2D, Supplementary Fig. 4). Under the optimized reaction conditions, no side adducts were observed with any amino acids regardless of the presence or absence of thiol. However, we observed that the N-terminus of the peptide behaved similarly to Lys, forming the pyrrole crosslink product **2d** with greater than 95% conversion only in the presence of both 4-ONE and butanethiol (Fig. 2D, Supplementary Fig. 4). Together, these findings establish that 4-ONE-mediated pyrrole formation is both cooperative and highly chemoselective, creating a uniquely controlled covalent linkage that is well suited for purposeful installation in peptide and protein settings.

Late-stage functionalization of peptides by incorporating pyrrole crosslinks

With this chemoselective reactivity in hand, we next asked whether 4-ONE could be used not only to reveal covalent connectivity, but also to install new function deliberately. We therefore explored 4-ONE-mediated pyrrole formation as a late-stage functionalization (LSF) strategy to diversify peptides rapidly and modulate biological activity[30–34]. To demonstrate this potential, the moderately cytotoxic peptide Ac-RGVKGPR[35] **1e** was functionalized with 4-ONE in the presence of distinct thiols encompassing diverse structural motifs; linear aliphatic thiols (with a hydroxy, carbonyl, or carboxyl group), a branched aliphatic thiol, and a thiol containing an aromatic group. This strategy generated a library of pyrrole-modified peptides **2e-2i**, each obtained with >95% conversion. To further demonstrate the preparative utility of this approach, pyrrole-modified peptides **2e-2i** were synthesized on 10 mg scale and isolated after HPLC purification in 41–47% yield (Fig. 2E, Supplementary Fig. 5). Next, to assess the impact of these modifications on cytotoxicity, we incubated these peptides (500 µM, 24 h) with MCF-7 cells (Fig. 2E, Supplementary Fig. 6). Pyrrole peptides **2e-2f** displayed cytotoxicity toward MCF-7 cells comparable to the parent peptide **1e**, whereas modified peptides **2g-2i** caused a significant enhancement in cell death, with **2i** exhibiting the greatest decrease in cell viability, >3 fold greater than parent peptide **1e**. Further dose-response analysis in MCF-7 cells revealed that **2i** induced substantial cytotoxicity at concentrations as low as 150 µM, representing a pronounced increase in potency relative to the unmodified peptide (Fig. 2E, Supplementary Fig. 6). Collectively, these findings highlight the power of this LSF method for introducing structure-activity relationship (SAR) diversity, providing a powerful approach for fine-tuning peptide bioactivity. This ability to install a stable pyrrole linkage in a residue-selective fashion suggested that the same chemistry might also be harnessed intramolecularly to impose peptide constraints through cyclization and stapling.

Macrocyclization and stapling of peptides via chemoselective cysteine-lysine crosslinking

We next sought to translate this chemoselective Cys-Lys linkage into a conformational tool by testing whether 4-ONE could drive efficient macrocyclization and stapling of peptides. A series of peptides, H_2N-YNDPFRC **3a**, Ac-RFGKGFC **3b**, Ac-KFPC **3c**, H_2N-WGLRC **3d**, and Ac-KWGMEGFRC **3e**, each containing both cysteine and lysine (or an N-terminal amine), were treated with 3 equiv. of 4-ONE in a NaP buffer:MeCN (1:1) mixture under optimized conditions. The reactions resulted in side-chain-to-side-chain or head-to-side-chain macrocycles **4a**–**4e** featuring a pyrrole moiety at the site of cyclization, achieving ≥95% conversion as judged by LC–MS/HPLC disappearance of the starting peptide and appearance of the dominant macrocycle peak (Fig. 3A, Supplementary Fig. 7). HPLC traces are shown as crude reaction mixtures; minor peaks are low-level background features of the crude mixture and are not interpreted as purified peptide impurities.

Building on this chemoselectivity, we extended the methodology to peptide stapling between identical residues. For Cys-to-Cys stapling, peptide Ac-DCSNCFR **5**, containing two cysteine residues located at the i and i + 3 positions was first treated with five equivalents of 4-ONE. After confirming Michael addition at both cysteines, we added 1 equivalent of either propane-1,3-diamine or butane-1,4-diamine in four portions at 2.5 h intervals. LC-MS analysis revealed >95% conversion to stapled products **6a** and **6b** irrespective of the linker length (Fig. 3B, Supplementary Fig. 8). For Lys-to-Lys stapling, peptide Ac-RKWFKLI **7** with lysines at the i and i + 3 positions was incubated with 4-ONE and either propane-1,3-dithiol or butane-1,4-dithiol, affording stapled peptides **8a** and **8b** containing two pyrrole crosslinks in >95% conversion (Fig. 3B, Supplementary Fig. 9).

Synthesis of pyrrole-crosslinks on solid support

To enable selective crosslinking at lysine residues while avoiding undesired Michael additions to cysteine within the same peptide and to achieve selective lysine modification in the presence of multiple lysines, we optimized the reaction conditions under solid-phase peptide synthesis (SPPS). Using a simple dipeptide GF **9** on a solid support with a free N-terminus, we systematically varied the equivalents of 4-ONE, butanethiol, and reaction time (Fig. 3C, Supplementary Fig. 10). A 57% conversion to the desired pyrrole product **10** at the N-terminus was obtained using 5 equiv. of 4-ONE and 15 equiv. of butanethiol in DMF for 12 h. Increasing the amount of 4-ONE to 10 equiv. or extending the reaction time to 24 h using 5 equiv. of 4-ONE, we were able to achieve >95% conversion to pyrrole product **10**.

Having established efficient conditions for forming selective crosslinks with lysine on solid support, we next applied this strategy to modify a Cys in the presence of a Lys residue. Selective deprotection of

https://doi.org/10.1038/s41467-026-74843-x

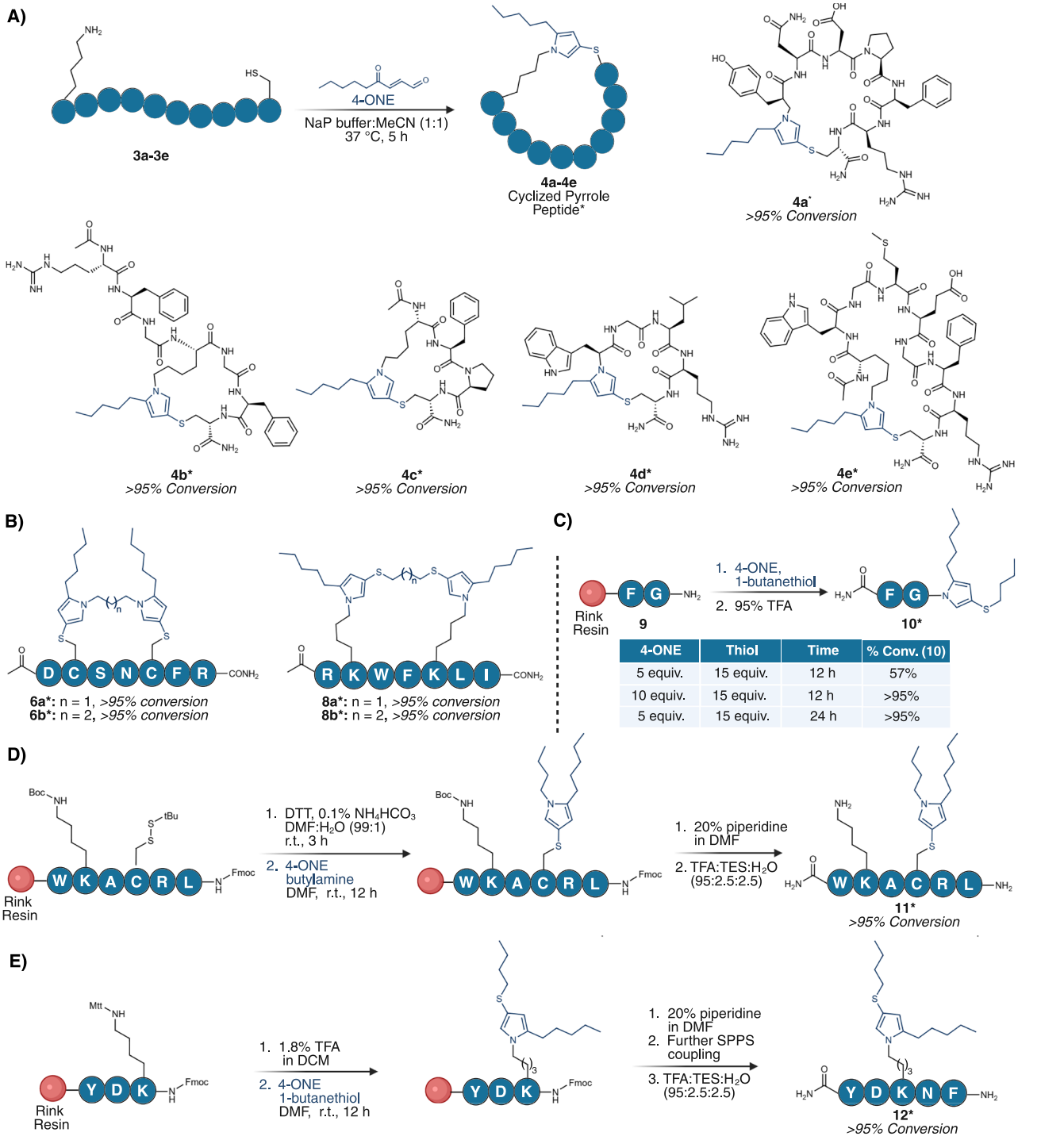

Fig. 3 | Application of 4-ONE as a selective covalent crosslinker for macrocyclization, stapling, and solid-phase functionalization. A Macrocyclization of peptides **3a**-**3e** containing Cys and Lys (or the N-terminus) using 4-ONE (3 equiv.) afforded side-chain-to-side-chain and head-to-side-chain macrocycles **4a**-**4e** with dominant product formation by crude LC–MS/HPLC analysis. **B** Stapling of peptides containing Cys (i, i + 3) or Lys (i, i + 3) residues was achieved using 4-ONE in combination with diamines or dithiols, affording stapled cysteine peptides **6a**-**6b** and stapled lysine peptides **8a**-**8b** with >95% conversion. **C** Solid-phase synthesis of pyrrole-modified peptides to enable selective functionalization of Cys or Lys residues in the presence of other amines/thiols. Initial optimization yielded N-terminal pyrrole peptide **10**. **D** Selective deprotection on solid support using Cys(StBu) yielded pyrrole peptide product **11** in the presence of Lys, with >95% conversion. **E** Selective deprotection on solid support using Lys(Mtt) yielded pyrrole peptide product **12** despite presence of N-terminal amine, again in >95% conversion. HPLC traces are crude reaction mixtures; product identity is confirmed by MS of the product peak/retention window (Supplementary Figs. 7–10). *Representation depicts one of the possible regioisomers generated by the 4-ONE cross-coupling. *Created in BioRender. Lab, R. (2026)* https://BioRender.com/kub4o7p.

Cys (StBu)[36] on solid support followed by reaction under optimized conditions yielded the pyrrole-modified peptide H_2N-LRCAKW **11** with >95% conversion (Fig. 3D, Supplementary Fig. 10). The pyrrole product remained stable under both Fmoc deprotection (20% piperidine, basic) and peptide cleavage (95% trifluoroacetic acid (TFA), acidic) conditions, confirming its robustness during solid-phase peptide synthesis. We then targeted selective lysine modification in the presence of N-terminal amine by deprotecting Lys(Mtt) and introducing

the 4-ONE pyrrole at the free Lys. Subsequent coupling of Asn and Phe prior to resin cleavage afforded the lysine pyrrole-modified product H_2N-FNKDY **12** in >95% conversion (Fig. 3E, Supplementary Fig. 10). The pyrrole linkage remained intact throughout Fmoc deprotection and coupling steps, underscoring its remarkable stability and compatibility with SPPS workflows. Together, these results establish 4-ONE-mediated pyrrole formation as a robust and orthogonal method for on-resin peptide modification, positioning the chemistry to move beyond peptide synthesis and into folded protein substrates.

Substrate scope for selective labeling of proteins using 4-ONE

Having established the selectivity, stability, and synthetic utility of the pyrrole linkage in peptides, we next asked whether the same chemistry could be deployed selectively on folded proteins. We selected myoglobin as a model system, which contains 19 lysine and no cysteine residues. Treating myoglobin with 8 equiv. of 4-ONE in the absence of thiol resulted in no modification, consistent with our earlier chemoselectivity studies on Cys-Lys crosslink peptides (Fig. 4A, Supplementary Fig. 11). Varying the equivalents of 4-ONE and thioglycolic acid (3-8 equiv.) at 37 °C in 4:1 NaP buffer:MeCN (pH 7.4) revealed that five equivalents of each reagent provided the most controlled labeling profile, with singly modified myoglobin predominating and no unmodified protein detected by LC-MS (Fig. 4A, Supplementary Fig. 11). Despite the presence of 19 lysines in myoglobin, pyrrole modification occurred only at a subset of residues under these conditions. LC-MS/MS analysis of the modified myoglobin (5 equiv. 4-ONE, thioglycolic acid) identified K45, K96, and K133 as the modified sites (Supplementary Fig. 11). The selective emergence of only a small subset of modified lysines suggested that 4-ONE does not label proteins indiscriminately but instead reports on privileged local environments that favor pyrrole formation. Next, we determined the stability of the pyrrole adduct across a range of pH values. The expected pyrrole-modified myoglobin species were retained after 24 h at 37 °C across pH 2.4–10.8, with no apparent new degradation products under the LC–MS conditions used (Supplementary Fig. 12), confirming its suitability for downstream applications such as affinity tagging, protein profiling, and mechanistic studies of metabolite-driven modifications.

With optimized reaction conditions (5 equiv. 4-ONE, thioglycolic acid) established for selective generation of singly modified myoglobin, we extended the strategy to a broad range of proteins, such as aprotinin, lysozyme (chicken and human), insulin, ubiquitin, ribonuclease A, cytochrome C, apo-transferrin, and β-lactoglobulin, with different molecular weights (5.8 kDa–79.5 kDa) and three-dimensional structures. Across this protein panel, LC-MS detected 4-ONE-derived pyrrole-modified species, with the number and relative abundance of modified species varying by substrate (Fig. 4B, Supplementary Fig. 13).

We next utilized this chemistry for selective modification of Cys by adding 20 mM dithiothreitol (DTT) to ribonuclease A to reduce its four disulfide bonds, followed by incubation with 4-ONE and glycine. LC-MS/MS analysis revealed formation of pyrrole adducts at four cysteine residues (C26, C40, C58, C65), confirming modification of the reduced cysteine residues under these conditions (Supplementary Fig. 14).

Finally, to enable downstream conjugation, we synthesized an alkyne-functionalized 4-ONE analogue (see Supplementary Fig. 15 for synthesis). Reaction of this analogue with myoglobin and thioglycolic acid led to near-complete consumption of unmodified myoglobin and formation of the corresponding alkyne-pyrrole adduct, facilitating subsequent click-based payload conjugation and proteomics labeling workflows[37–39] (Supplementary Fig. 16).

This chemoselective labeling strategy remained effective even in complex protein environments. We therefore proceeded to ask whether this selectivity would be retained in complex biological mixtures, where competing nucleophiles, endogenous thiols, and broad proteome diversity provide a more stringent test of the chemistry. In T-47D cell lysates, we performed dose-dependent modification of Cys or Lys residues by incubating with 4-ONE and either propargylamine or alkyne thiol, followed by fluorophore tagging with Cy5 azide. A dose-dependent increase in fluorescence was observed in both cases (Fig. 5A, Supplementary Fig. 17).

We next demonstrated the incorporation of bulky fluorophores into 4-ONE-derived pyrroles. Treatment of T-47D lysate with 250 μM 4-ONE and 250 μM Az680 amine dye resulted in robust cysteine labeling detected by in-gel fluorescence, whereas no signal was observed in controls lacking 4-ONE or Az680 (Supplementary Fig. 18). To further illustrate the orthogonality of the chemistry, we performed dual labeling of lysine in T-47D cell lysate by combining thiol-FITC with 4-ONE alkyne, followed by conjugation of Cy5 azide to the pyrrole using Copper-Catalyzed Azide-Alkyne Cycloaddition (CuAAC)[39]. In-gel analysis verified precise, orthogonal incorporation of both FITC and Cy5 fluorophores onto proteins (Fig. 5B, Supplementary Fig. 18). Together, these results show that 4-ONE-mediated pyrrole formation remains selective and chemically addressable in complex lysates, motivating a proteome-wide analysis of which residues and protein classes are preferentially captured under conditions of increasing aldehyde stress.

Investigation of proteins prone to 4-ONE modification via dose-dependent proteomic profiling

To define the proteomic consequences of this chemistry, we next implemented a dose-dependent profiling platform in T-47D human breast cancer cells. This approach enabled systematic identification of lysine and cysteine residues preferentially modified as 4-ONE exposure increased, thereby linking residue-level reactivity to oxidative-stress-associated proteotoxicity[39–41].

For lysine labeling, cell lysates were incubated with varying concentrations of 4-ONE and thioglycolic acid (50–1000 μM), while cysteine labeling was probed using 4-ONE and glycine under identical conditions (Fig. 5C, Supplementary Figs. 19–20). LC–MS/MS analysis revealed a clear dose-dependent increase in pyrrole-lysine modifications, rising from 53 proteins at 50 μM to 162 proteins at 1000 μM. Under the lysine-labeling conditions, thioglycolic acid ($\leq$1 mM) is present in large excess relative to accessible free cysteines in the lysate and rapidly scavenges 4-ONE, thereby suppressing direct Michael-type addition to protein cysteines. Consistent with this model, LC–MS/MS analysis of these samples did not detect cysteine–4-ONE Michael adducts or other cysteine-associated 4-ONE modifications above background. In contrast, pyrrole-cysteine labeling exhibited only a modest increase, from 23 proteins at 50 μM to 33 proteins at 1000 μM. Heat map visualization confirmed a progressive elevation in the modified/unmodified ratio for lysine sites, whereas cysteine reactivity did not change as substantially moving from 50 to 1000 μM (Supplementary Figs. 19–20). Sequence motif analysis (pLogo)[42] of modified sites observed at all the doses showed that both Lys and Cys modifications were enriched in hydrophobic sequence environments, with Ile and Leu strongly overrepresented near Lys-modified sites, and Leu, Val, and Ile prevalent near Cys-modified sites (Fig. 5C, bottom). Structural mapping of the 57 Lys and 16 Cys residues classified as "hyperreactive," defined here as residues modified under all tested 4-ONE concentration conditions, revealed that most were located in hydrophobic pockets (Fig. 5C, Supplementary Figs. 19–20). These findings suggest that the 4-ONE derived pyrrole is promoted in hydrophobic microenvironments. We propose that 4-ONE-derived pyrrole formation is kinetically and thermodynamically favored in hydrophobic microenvironments, where water exclusion stabilizes the intermediate enamine-imine and promotes irreversible cyclization to pyrrole. In contrast, polar aqueous environments favor reversible Schiff-base formation, leading to fewer persistent adducts. This explains why lysine residues embedded in hydrophobic environments,

https://doi.org/10.1038/s41467-026-74843-x

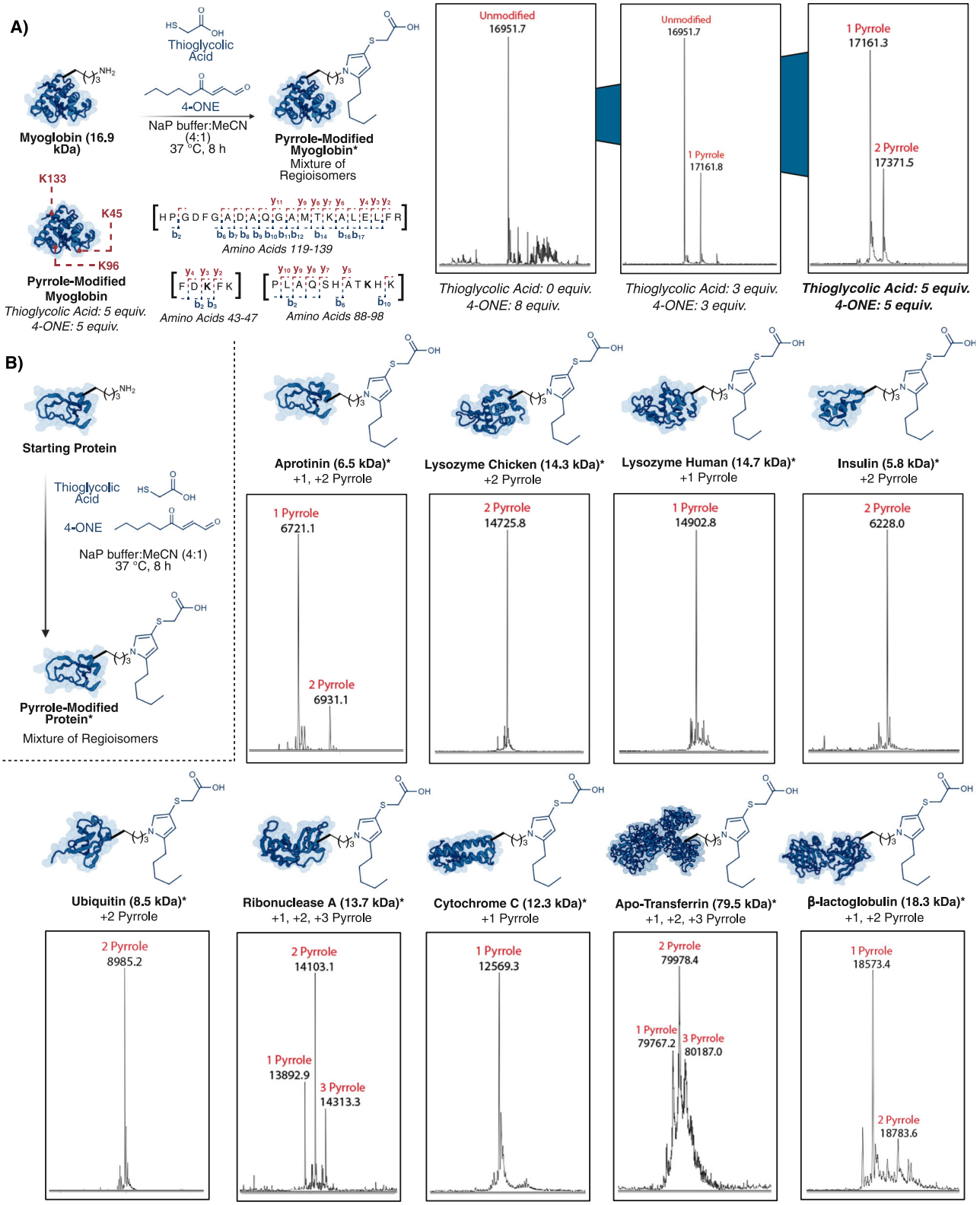

Fig. 4 | Selective labeling of proteins using 4-ONE. A Optimization of 4-ONE myoglobin modification. Myoglobin showed no reactivity toward 4-ONE alone; however, in the presence of thioglycolic acid (5 equiv.) and 4-ONE (5 equiv.), the reaction yielded a product bearing one to two pyrrole modifications. LC-MS/MS analysis of the modified protein identified a subset of hyperreactive lysine residues (K45, K96, and K133) as primary labeling sites. **B** Substrate scope of 4-ONE-mediated Lys modification across proteins of varying size and three-dimensional structure (5.8 kDa–79.5 kDa). Reactions conducted with 5 equiv. 4-ONE and 5 equiv. thioglycolic acid showed substantial pyrrole modification across structurally distinct proteins, with substrate-dependent product distributions. *Representation depicts one of the possible regioisomers generated by the 4-ONE cross-coupling. *Created in BioRender. Lab, R. (2026)* https://BioRender.com/hrtqpqv.

https://doi.org/10.1038/s41467-026-74843-x

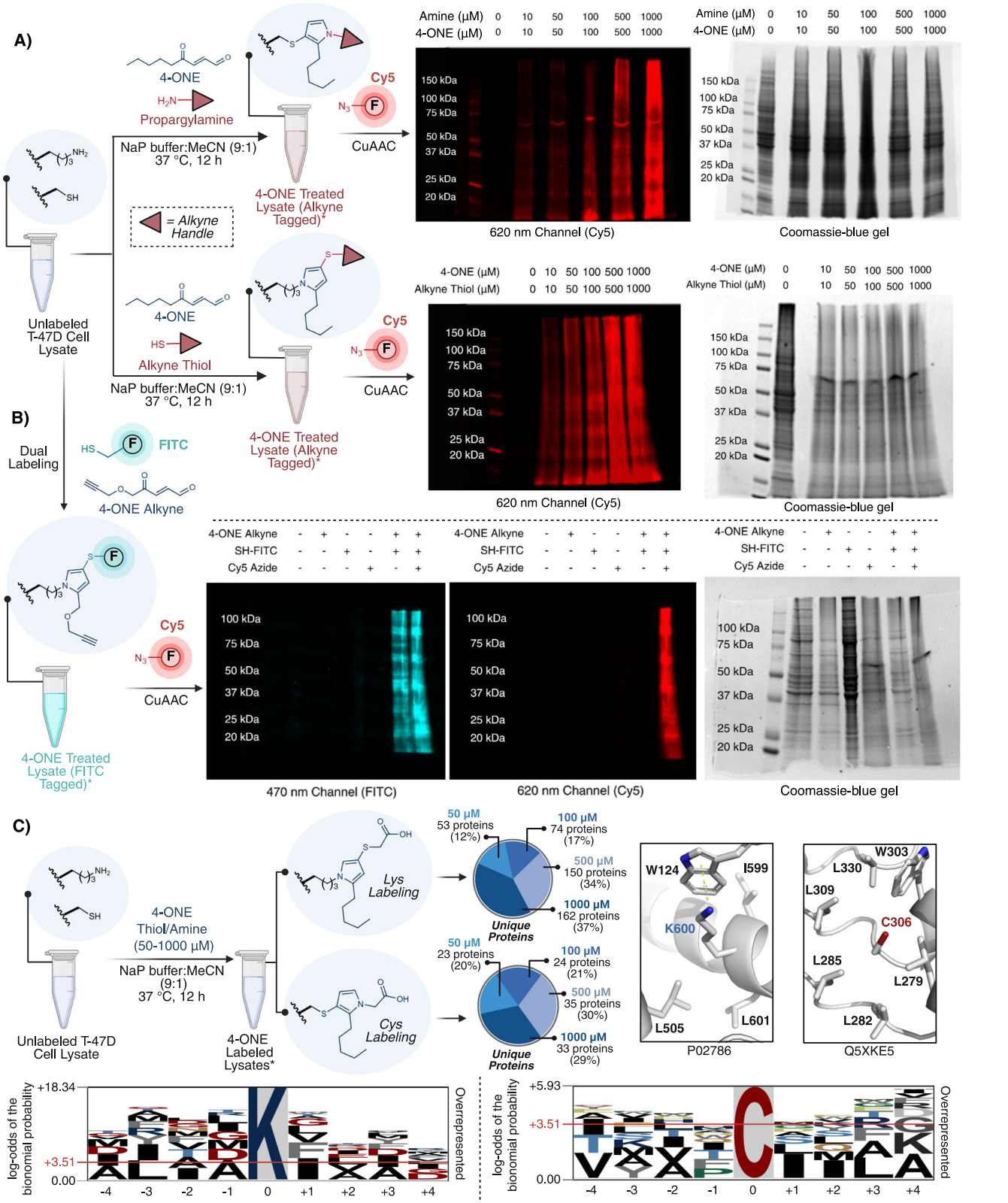

often located at protein–protein interfaces or within folded cores, exhibit enhanced modification efficiency.

The weaker dose response of cysteine labeling likely arises from competition with endogenous thiols (e.g., glutathione) and the higher intrinsic nucleophilicity and reactivity of thiols, which results in rapid, low-level saturation at modest 4-ONE concentrations. In contrast, lysine modification proceeds through a slower, cooperative process that accumulates progressively with increasing aldehyde dose, reflecting distinct kinetic regimes of 4-ONE reactivity with soft (Cys) vs. hard (Lys) nucleophiles.

Gene Ontology (GO) enrichment analysis[43,44] further distinguished functional consequences of these reactivities. Lysine-modified proteins were enriched in categories associated with protein folding, ribosome structure, and nucleic acid binding, implicating perturbation

Fig. 5 | Chemoselective and orthogonal protein labeling in cell lysates using 4-ONE. A Dose-dependent labeling of T-47D cell-lysate proteins using 4-ONE in the presence of propargylamine (for Cys labeling) or an alkyne thiol probe (for Lys labeling). Labeled proteins were visualized by in-gel fluorescence following Cy5-azide click conjugation, showing concentration-dependent increases in signal intensity. These experiments were repeated ($n = 3$ biological replicates) with similar results. **B** Orthogonal dual labeling of lysate proteins by sequential modification of lysines with 4-ONE alkyne and cysteines with FITC-thiol, followed by Cy5 azide conjugation. In-gel fluorescence at 470 nm (FITC) and 620 nm (Cy5) confirmed selective, simultaneous incorporation of multiple functional tags into distinct protein populations. This experiment was repeated ($n = 3$ biological replicates) with similar results. **C** Proteomic profiling analysis revealed a dose-dependent increase of pyrrole-lysine and modest increase in pyrrole-cysteine adducts ($n = 2$ biological replicates). Sequence-motif analysis indicated preferential modification of Lys and Cys residues flanked by hydrophobic amino acids. Structural mapping of 57 hyperreactive Lys and 16 hyperreactive Cys sites consistently detected across all concentration conditions revealed that most reactive residues are positioned in solvent-accessible or partially buried hydrophobic pockets (Lys-labeled site shown in blue and Cys-labeled site shown in red). Source data are provided as a Source Data file. *Representation depicts one of the possible regioisomers generated by the 4-ONE cross-coupling. *Created in BioRender. Lab, R. (2026)* https://BioRender.com/3fci7td.

of translational and genomic stability (Supplementary Figs. 19–20). Cysteine-modified proteins were associated with antioxidant activity, thioredoxin reductase activity, and cytoskeletal organization, implicating redox imbalance and structural destabilization (Supplementary Figs. 19–20). Collectively, these findings reveal that 4-ONE preferentially targets hydrophobic residues within proteins critical for proteostasis and redox regulation, providing a chemical rationale for aldehyde-mediated cytotoxicity under lipid peroxidation stress.

Because the same microenvironments that favor persistent pyrrole formation could also promote covalent bridging between nearby cysteine and lysine residues, we next asked whether 4-ONE can directly generate structurally meaningful protein crosslinks.

4-ONE as a chemoselective covalent crosslinker for identification of protein crosslinks

Having established that 4-ONE selectively generates stable Cys-Lys pyrrole linkages, we next asked whether this chemistry could extend from site modification to bona fide protein crosslinking under oxidative-stress-relevant conditions[45]. As an initial demonstration, we incubated creatine kinase (43.0 kDa), containing a single free Cys at position 282, with myoglobin (16.9 kDa) and 4-ONE. Gel electrophoresis revealed the appearance of higher-order crosslinked species, including a ~ 60 kDa band. This band was excised and analyzed by in-gel digestion followed by LC–MS/MS, which identified peptides from both creatine kinase and myoglobin, supporting 4-ONE–mediated hetero-crosslink formation between distinct proteins (Supplementary Fig. 21).

To investigate 4-ONE crosslinking in situ, live cells were treated with increasing concentrations of 4-ONE alkyne (50–250 μM) for 4 h. No significant cytotoxicity was observed at these doses (Supplementary Fig. 22). Cells exposed to 250 μM 4-ONE alkyne were fixed and subjected to Cu-catalyzed azide–alkyne cycloaddition (CuAAC) with Cy5 azide. Strong intracellular fluorescence, including nuclear localization, occurred exclusively in treated cells, confirming efficient intracellular protein crosslinking (Fig. 6A, Supplementary Fig. 23). To identify the proteome-wide targets of 4-ONE crosslinking, we performed chemoproteomics using biotin-azide-enriched lysates from 250 μM 4-ONE alkyne-treated T-47D cells across three independent biological replicates to compare against identically processed, non-specific binding control samples ($n = 3$). Proteins were considered enriched if they were detected in at least two replicates and showed greater than 4-fold enrichment relative to controls. To confirm that enrichment resulted from bona fide crosslinks and not amine-reactive monolinks, 4-ONE-alkyne-treated cell lysates were incubated with 250 μM Az680 amine dye. Subsequent SDS-PAGE of these lysates showed no detectable labeling by in-gel fluorescence. In contrast, CuAAC modification of the same lysates with 250 μM Cy5 azide produced robust protein labeling, confirming the presence of pyrrole crosslinks and the absence of amine-reactive monolinks (Supplementary Fig. 23). Overall, this controlled, replicated workflow identified 1618 high-confidence, enriched proteins (Fig. 6B). Gene Ontology analysis revealed enrichment of proteins involved with RNA-binding, ribonucleoprotein complex components, focal adhesion, cadherin-binding, and the proteasome, which aligns with preferential 4-ONE reactivity at hydrophobic protein-protein interfaces. This distribution closely parallels that reported in a prior site-specific chemoproteomic study of 4-ONE adducts, which identified overlapping categories, including RNA binding, cadherin-mediated cell adhesion, mRNA splicing, and ribonucleoprotein complexes[28]. Consistent with this overlap, 129 of 183 proteins (71%) from that study were also significantly enriched in our dataset, including CFL1, GAPDH, TXN, EEF2, HSP90AB1, ACTN1, and PARK7, providing strong cross-study validation. The orthogonal proteins identified in our dataset represent potentially novel 4-ONE targets that warrant future investigation.

COSMIc: late-stage generation of mass-cleavable Cys-Lys pyrrole crosslinks for structural proteomics

While 4-ONE efficiently forms stable Cys-Lys pyrrole crosslinks, a key analytical challenge remains: the lack of an intrinsic, MS-cleavable moiety. Crosslinkers that are cleavable within the mass spectrometer have been shown to improve peptide backbone fragmentation and can generate diagnostic fragment ions to distinguish bona fide crosslinks from gas-phase associated peptides[46]. To overcome this limitation, we developed COSMIc (Crosslink Oxidation to Sulfoxide for Mass-Cleavable Interactomics): a late-stage oxidation strategy that converts stable 4-ONE-derived Cys-Lys pyrrole crosslinks into MS-cleavable sulfoxides. Upon collision-induced dissociation (CID), these oxidized linkages fragment more productively, producing more assignable backbone fragments from each peptide, including link-site-containing fragments, thereby improving peptide identification, residue-pair assignment, and crosslink scores[47,48]. Distinct from pre-installed, synthetic sulfoxide linkers[49], COSMIc converts an endogenous-metabolite-derived thioether into an MS-cleavable bond only after covalent capture has occurred, directly linking oxidative-stress electrophile chemistry to residue-pair mapping.

To validate this concept, we first examined model peptides containing either Lys or Cys. Reaction of Ac-FKALRNW with 4-ONE and 1-butanethiol produced pyrrole adduct **13**, which upon oxidation with H_2O_2[50] yielded sulfoxide **14** that fragmented to the sulfenic acid product **15**. Dehydration of the sulfenic acid product was observed, consistent with prior literature[21] (Fig. 7A, Supplementary Fig. 24). Similarly, Ac-GRGDSPC treated with 4-ONE and butylamine afforded pyrrole **16**, which upon oxidation generated sulfoxide **17** and the subsequent dehydroalanine **18** upon fragmentation (Fig. 7A, Supplementary Fig. 25). These results establish that COSMIc generates distinct and residue-specific mass fingerprints: sulfenic acid for lysine and dehydroalanine for cysteine.

To demonstrate simultaneous readout of both linked residues, a lysine-containing peptide, Ac-FKALRNW, and a cysteine-containing peptide, Ac-GRGDSPC, were crosslinked using 4-ONE alkyne to generate the two-peptide crosslinked product **S3**, which was isolated in 68% yield. Oxidation of **S3** then afforded the sulfoxide-containing crosslinked product **19**, isolated in 79% yield. Next, MS/MS fragmentation dissociated **19** into its constituent peptides, each bearing the

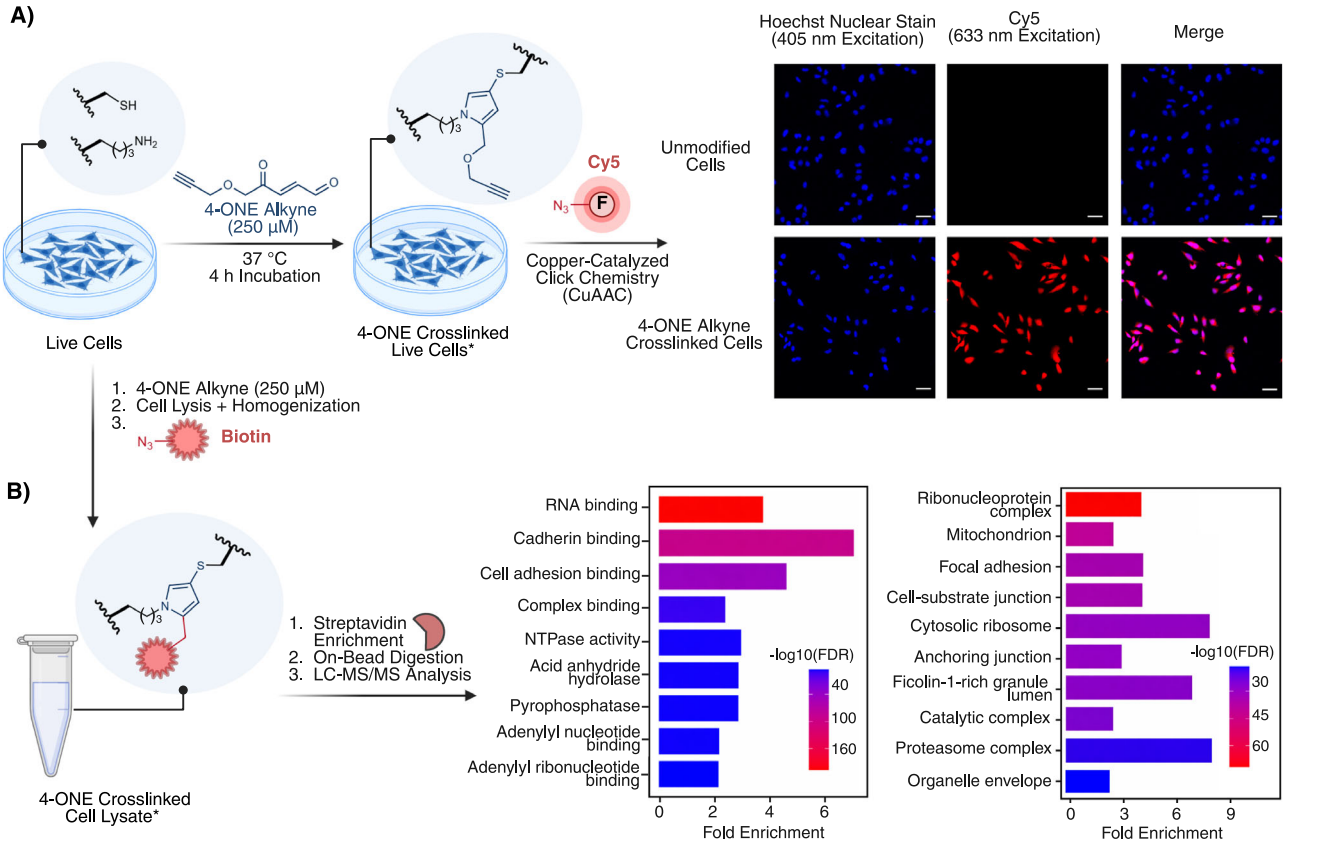

Fig. 6 | Identification of 4-ONE-mediated protein crosslinks in cellular systems. **A** Live cells treated with 4-ONE alkyne or vehicle (DMSO), fixed and subjected to CuAAC labeling with Cy5 azide, showed strong intracellular fluorescence colocalizing with Hoechst-stained nuclei, confirming intracellular protein crosslinking. This experiment was repeated ($n = 3$ biological replicates) with similar results. Scale bar = 50 µm. **B** Proteomic profiling of biotin-azide-enriched lysates from 250 µM 4-ONE alkyne-treated T-47D cells ($n = 3$ biological replicates) compared against matched non-specific binding controls ($n = 3$ biological replicates) identified 1618 high-confidence enriched proteins. Live-cell labeling was carried out in fully aqueous buffered media without any organic cosolvent. Proteins were captured by affinity enrichment and processed by on-bead digestion prior to LC–MS/MS analysis, which increases sensitivity relative to unenriched global proteomic workflows such as those seen in Fig. 5. Gene Ontology analysis (Molecular Function and Cellular Component) of enriched proteins revealed significant enrichment of RNA-binding proteins and ribonucleoprotein complex components, as well as focal adhesion, cadherin-binding proteins, and proteasome subunits, consistent with 4-ONE reactivity at hydrophobic protein-protein interfaces. Source data are provided as a Source Data file. *Representation depicts one of the possible regioisomers generated by the 4-ONE cross-coupling. *Created in BioRender. Lab, R. (2026)* https://BioRender.com/vj360bw.

expected COSMIc cleavage product: sulfenic acid on the Lys-containing peptide (Ac-FKALRNW) **20** and dehydroalanine on the Cys-containing peptide (Ac-GRGDSPC) **18** (Fig. 7B, Supplementary Fig. 26). In summary, we demonstrate that COSMIc affords accurate identification of both peptide- and residue-pairs for simple peptide systems.

Encouraged by these results, we next applied COSMIc to modified proteins. We reacted myoglobin with 4-ONE and thioglycolic acid and subsequently oxidized the crosslinks with H_2O_2 to yield the MS-cleavable pyrrole sulfoxides. LC-MS/MS identified the characteristic sulfenic acid at 14 of the 15 modified lysines (Fig. 7C, Supplementary Fig. 27). To probe intra-protein crosslinks, creatine kinase containing a single free cysteine (C282) was modified with 4-ONE. COSMIc enabled direct detection of dehydroalanine at C282 together with sulfenic acid at six lysines, revealing multiple intra-protein Cys-Lys crosslinks within a single protein (Fig. 7D, Supplementary Fig. 28). These data establish that COSMIc is effective not only for model peptides, but also in complex protein contexts where site-resolved readout of 4-ONE-derived connectivity is required.

Together, these findings establish COSMIc as a site-resolved readout for metabolite-derived Cys-Lys connectivity and set the stage for testing whether such crosslinks can report on residue-pair geometry within native macromolecular assemblies.

4-ONE as a structurally informative, MS-cleavable crosslinker

Having established COSMIc in model peptides and purified proteins, we next tested whether 4-ONE-derived crosslinks could be resolved in a native macromolecular assembly. Based on our enriched protein data, 4-ONE crosslinks were prevalent on proteasomal subunits (Fig. 6B). Accordingly, we chose to assay COSMIc on the human 26S proteasome for several additional reasons: its architecture is well defined, it contains multiple solvent-accessible Cys and Lys residues across a megadalton-scale assembly, and it provides a stringent benchmark for whether a compact Cys–Lys crosslinker can recover residue-pair restraints compatible with native structure[51,52]. Human 26S proteasomes were isolated through pulldown of biotin-tagged RPN1/PSMD2, a subunit of the 19S regulatory particle, followed by in vitro crosslinking with 4-ONE[53]. Where indicated, crosslinked proteasomes were treated with H_2O_2 to convert the 4-ONE-derived pyrrole linkage into the corresponding sulfoxide prior to digestion and LC–MS/MS analysis (Fig. 8A, Supplementary Fig. 29).

We identified 27 and 68 unique Cys–Lys residue pairs at a 5% residue-pair false-discovery rate (FDR) for non-oxidized and peroxide-oxidized 4-ONE crosslinks, respectively. This corresponds to 20 and 61 intra-subunit and 7 and 7 inter-subunit crosslinks, for non-oxidized and peroxide-oxidized 4-ONE crosslinks, respectively. To evaluate whether these crosslinks report on native proteasome architecture, we mapped

https://doi.org/10.1038/s41467-026-74843-x

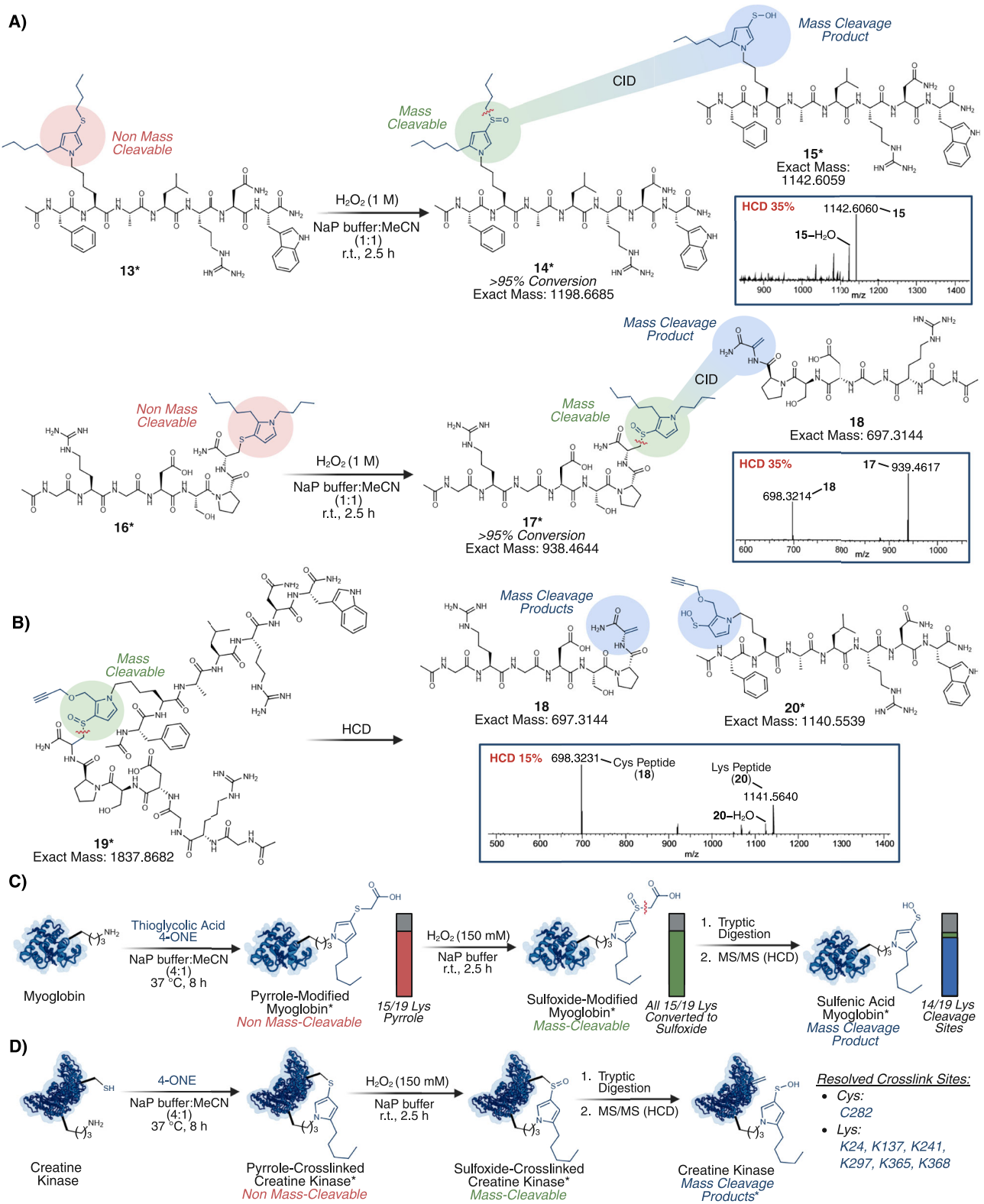

the identified residue pairs onto a high-resolution structure of the human 26S proteasome, PDB: 6MSE (Fig. 8B-C, Supplementary Fig. 29)[51]. 24 of 58 (41%) mapped crosslinks fell within 15 Å for Cα–Cα distances, consistent with the expected span of the 4-ONE-derived Cys–Lys pyrrole linkage and local side-chain flexibility. This represents 24 of 125 (19%) of all the surface-accessible Cys and Lys residue-pairs within that distance on this proteasome structure. 90% of crosslinks were found within a 35 Å Cα–Cα distance, consistent with the known conformational mobility of the 19S regulatory particle[54]. At a 5% residue-pair FDR, the overall distance distribution is therefore compatible with structurally informative crosslinking of a flexible native assembly. Notably, in the more rigid coupling interface between the 19S regulatory particle and the 20S core particle, 4-ONE captures two residue-pair crosslinks between ATPase subunit PRS6A/PSMC3/RPT5 and PSA1/PSMA1/a6, in both the oxidized and non-oxidized datasets (Fig. 8D). These data provide orthogonal support that 4-ONE can

Fig. 7 | COSMIc: late-stage generation of mass-cleavable 4-ONE-derived Cys–Lys crosslinks. A Oxidation of 4-ONE derived Lys-Cys pyrrole crosslinks to sulfoxides on peptides Ac-FKALRNW and Ac-GRGDSPC enabled predictable HCD-MS/MS fragmentation, yielding sulfenic acid (-SOH) from Lys adducts and dehydroalanine from Cys adducts. Dehydration of sulfenic acid was observed, consistent with previous literature reports[21]. **B** Identification of mass cleavage scars on both Lys and Cys by crosslinking peptides Ac-FKALRNW and Ac-GRGDSPC using 4-ONE alkyne, followed by oxidation of the pyrrole crosslink to sulfoxide. HCD–MS/MS enabled full fragmentation of sulfoxide peptide **19** to two peptides **18** and **20** with sulfenic acid on Lys (dehydration observed) and dehydroalanine on Cys. **C** Application of COSMIc to site-resolved readout of oxidized 4-ONE-derived lysine modifications on myoglobin. Myoglobin modified with 4-ONE and thioglycolic acid (8 equiv. each, modification identified at 15 of 19 Lys) were oxidized to sulfoxides (oxidation observed at all modified sites), with fragmentation revealing sulfenic acid at 14 Lys sites. **D** Application of COSMIc to determine intra-protein Cys–Lys crosslinks on creatine kinase, in which dehydroalanine at C282 and sulfenic acid formation at six lysines reveal multiple site-resolved intra-protein linkages. Source data are provided as a Source Data file. *Representation depicts one of the possible regioisomers generated by the 4-ONE cross-coupling. *Created in BioRender. Lab, R. (2026)* https://BioRender.com/j0e478m.

capture biologically relevant proteasome-associated contacts, rather than only abundant intra-complex proximities.

We next asked whether peroxide oxidation improved the interpretability of 4-ONE-crosslinked spectra. Previous work has demonstrated that MS-cleavable crosslinkers improve crosslinking-MS identification, primarily by increasing peptide-backbone fragmentation, rather than by diagnostic cleavage products alone. MS-cleavability generates shorter stub-containing fragments, increases matched b- and y-type ions, improves sequence coverage, and raises crosslink-spectrum-match scores[46]. The resulting A/T-type products can also support post-search filtering to increase identifications at a fixed FDR[55]. Consistent with this principle, peroxide oxidation converts the 4-ONE-derived pyrrole/thioether linkage into the corresponding sulfoxide, enabling more productive HCD fragmentation and improving assignment of both linked peptides (Fig. 8E, Supplementary Fig. 29). A representative crosslinked spectrum illustrates this gain in interpretability: the non-oxidized precursor corresponding to peptides from PRS10, containing crosslinked residues Lys-168 and Cys-193, is fragmented via HCD to generate only standard b- and y-ions, in addition to b- and y-ions that contain the intact crosslink and conjugate peptide (Fig. 8F, upper panel). Comparatively, this same peptide- and residue-pair in the peroxide-oxidized dataset generates many of these same fragment ions, in addition to fragment ions matched to dehydration of the sulfenic acid from the Lys side ("[T]") and corresponding dehydroalanine on the Cys side ("[A]"), resulting in improved peak annotation (Fig. 8F, lower panel). Notably, the sulfenic acid fragment ion is exclusively detected in its dehydrated form under these acquisition parameters. Across the dataset, H_2O_2 oxidation increased unique crosslinked spectrum matches (CSMs) from 110 to 202, unique residue pairs from 27 to 68, and protein-protein interactions from 17 to 30, at a 5% residue-pair FDR.

These results extend COSMIc from model systems to native structural proteomics. 4-ONE-derived crosslinks report on residue proximities compatible with the architecture and conformational flexibility of the human 26S proteasome, while peroxide-induced sulfoxide formation provides the fragmentation behavior needed for confident crosslinking-MS analysis. This establishes 4-ONE as a compact Cys–Lys crosslinker whose chemistry can be coupled to oxidation-dependent MS cleavage to improve residue-pair assignment in endogenous protein complexes.

Overall, this work redefines the lipid peroxidation product 4-ONE as a covalent MS-cleavable crosslinker that irreversibly links cysteine and lysine through a chemoselective, multi-step mechanism. By repurposing this reactive metabolite into a defined chemical platform, we uncover a unique mechanism involving highly selective cyclization of Cys and Lys to form pyrrole linkages. This chemistry proceeds under physiological conditions and can be deployed for late-stage peptide functionalization, macrocyclization, stapling, selective protein labeling, and proteome-wide profiling of hyperreactive sites.

Advances in crosslinking-MS workflows have allowed for accurate detection of this metabolite-derived linkage, establishing 4-ONE as a structurally informative crosslinking modality. Through COSMIc, late-stage oxidation converts stable pyrrole linkages into MS-cleavable sulfoxides that assist assignment of linked residue-pairs through diagnostic sulfenic acid and dehydroalanine products. Application to the human 26S proteasome shows that these crosslinks are consistent with native architecture, and that sulfoxide formation markedly improves fragment assignment and residue-pair confidence in crosslinking-MS analysis.

Together, these findings reposition 4-ONE from a by-product of oxidative stress to a metabolite-derived crosslinking platform for covalent mapping, structural proteomics, and interactome analysis. More broadly, they show how endogenous electrophile chemistry can be converted from a poorly traceable mark of damage into a site-resolved source of covalent and structural information.

Methods

Synthesis of 4-ONE

1-Octen-3-ol (racemic mixture) (1.23 mL, 8 mmol, 1 equiv.) and acrolein dimethyl acetal (2.84 mL, 24 mmol, 3 equiv.) were dissolved in dry DCM (10 mL) in a 50 mL round-bottom flask. Hoveyda-Grubbs catalyst (12.5 mg, 0.02 mmol, 2.5 mol%) was added to the stirring mixture. Half of the catalyst was added immediately, and the other half was added after 5 h. The reaction was stirred for 24 h at room temperature then diluted with DCM (20 mL). The organic layer was washed with brine (3 × 25 mL), dried over Na_2SO_4, and then adsorbed onto silica. Flash column chromatography yielded crude (E)-1,1-dimethoxynon-2-en-4-ol (racemic mixture) as a clear liquid (1.15 g).

Crude (E)-1,1-dimethoxynon-2-en-4-ol (racemic mixture) (1.15 g, 5 mmol, 1 equiv.) was then dissolved in 15 mL of acetone:H_2O (2:1). Pyridinium p-toluenesulfonate (125.7 mg, 0.5 mmol, 10 mol%) was added to the reaction mixture. The reaction was stirred at room temperature for 2 h, after which acetone was evaporated. EtOAc (20 mL) was added, and the organic layer was extracted with brine (3 × 25 mL), dried over Na_2SO_4, and then adsorbed onto silica. Purification by column chromatography (1:3 EtOAc:Hex eluent) yielded 4-hydroxynonenal as a viscous and clear light yellow liquid (723 mg).

4-hydroxynonenal (625 mg, 4 mmol, 1 equiv.) was dissolved in DCM (15 mL) in a 50 mL round-bottom flask. Dess-Martin periodinane (2.21 g, 5.2 mmol, 1.4 equiv.) was added to the reaction mixture, which was allowed to stir for 1.5 h. Upon completion by TLC, the reaction mixture was diluted with DCM (15 mL), washed with brine (3 × 25 mL) in a 125 mL separatory funnel, dried over Na_2SO_4, and then adsorbed onto silica. Purification by column chromatography (1:7 EtOAc:Hex eluent) furnished 4-oxononenal as a light yellow solid (537 mg).

General procedure for peptide modification with 4-ONE

Peptide containing lysine and/or cysteine (1 mg, 1 equiv.) was dissolved in 480 μL of 1:1 10 mM NaP buffer (pH 7.4):ACN in a 1" dram vial. 4-ONE (3 equiv.) and external thiol or amine (if desired) was added from freshly prepared stock solutions (10 μL each in 1:1 NaP buffer (pH 7.45):ACN). The mixture was stirred at 37 °C for 5 h, after which the reaction was analyzed using (0–80% B over 30 min, solvent B: 0.1% formic acid in MeCN, flow rate: 1 mL/min) and MS to determine the conversion to pyrrole-containing peptides.

https://doi.org/10.1038/s41467-026-74843-x

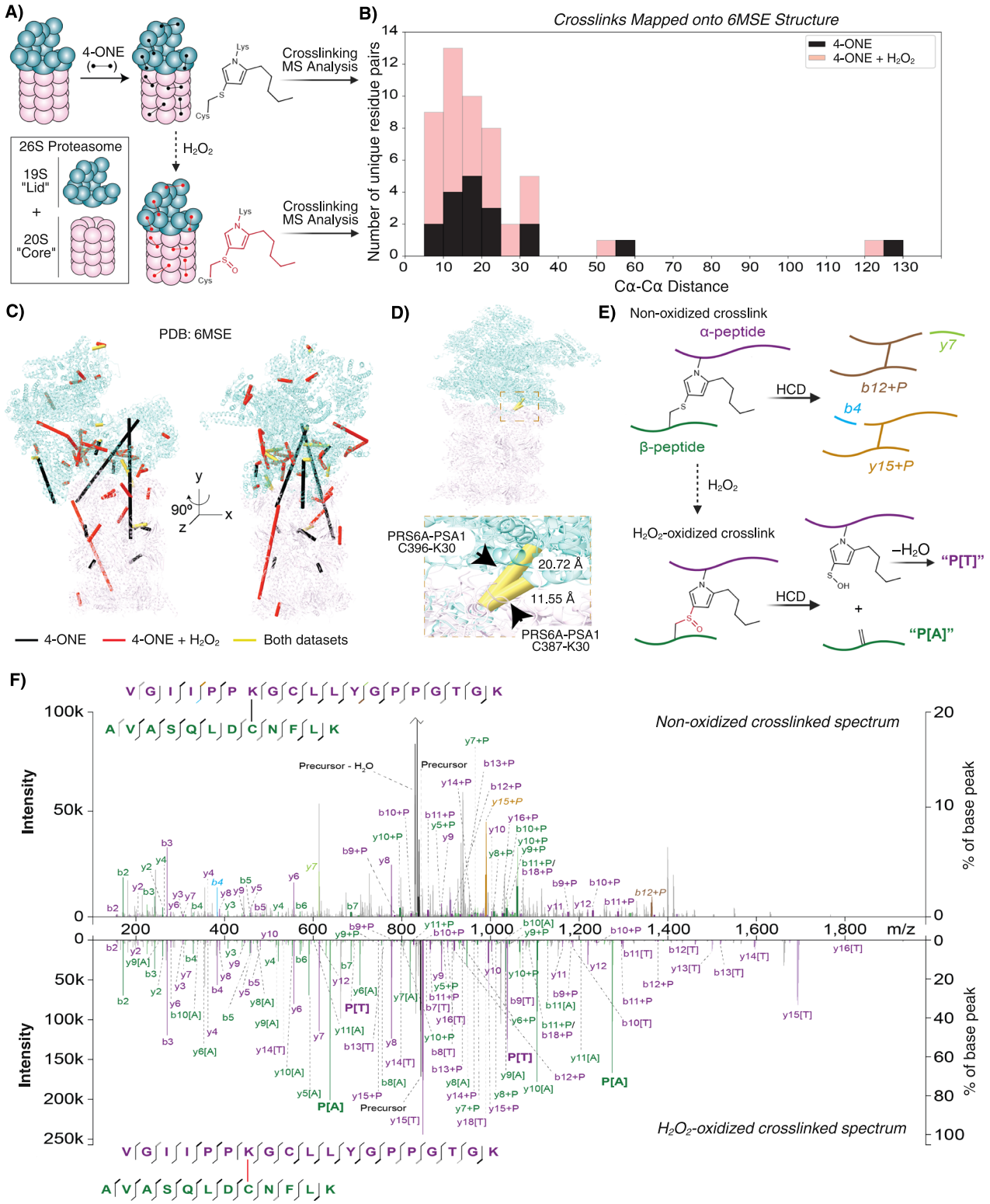

Cell viability analysis of peptides 2e-2i

MCF-7 cells (Catalog #HTB-22) were grown in 60 ×15 mm Nunclon™ dishes and allowed to adhere overnight in an incubator at 37 °C, 5% CO_2. Stock solutions of **1e** and **2e-2i** were prepared in DMSO (50 mM) then diluted to the final concentration in 3 mL of media. Vehicle controls were treated with an equivalent dosage of DMSO in media. Cells were placed in an incubator for 24 h, then analyzed by flow cytometry using AV/PI staining (FITC Annexin V purchased from Biolgened, Catalog No. 640945, Lot No. B404229). Data is an average of 3 replicates analyzed on separate days using different passage number of cells. One way ANOVA was used to determine significance. All error bars represent mean ± standard deviation.

General procedure for modification of proteins

Protein (2 mg, 1 equiv.) was dissolved in 475 μL of 10 mM NaP buffer (pH 7.4):ACN (4:1). 4-ONE (5 equiv.) in 5 μL ACN stock solution and thioglycolic acid (5 equiv.) in 20 μL H_2O stock solution were then added to the mixture. The reaction was stirred at 37 °C for 8 h, after which the

Fig. 8 | Structural validation and peroxide-enabled MS-cleavability of 4-ONE-derived crosslinks in the human 26S proteasome. A Human 26S proteasome was isolated by pulldown of biotin-tagged RPN1 (PSMD2) subunit[53]. The 26S proteasome comprises the 19S regulatory particle (teal) and 20S core particle (pink). RPN1 pulldowns were crosslinked in vitro with 4-ONE, optionally oxidized with H_2O_2 to generate the MS-cleavable sulfoxide crosslink (red; non-oxidized crosslink shown in black), and analyzed by crosslinking-MS. **B** Stacked histogram showing unique residue pairs plotted by Cα–Cα distance on the 6MSE structure. Non-oxidized 4-ONE crosslinks are shown in black and peroxide-oxidized crosslinks in light red. **C** 4-ONE crosslinks mapped onto the 26S proteasome structure (PDB: 6MSE)[51] as ChimeraX pseudobonds, with non-oxidized crosslinks in black, oxidized crosslinks in red, and shared crosslinks in gold. The right structure is rotated 90° clockwise about the y-axis. **D** The same 6MSE structure, rotated 240° about the y-axis, showing only 19S–20S interface crosslinks shared between datasets. The lower panel shows a zoomed-in view of the boxed interface region, illustrating two residue pairs and their Cα–Cα distances. **E** HCD of non-oxidized 4-ONE crosslinks generates conventional b- and y-ions containing the intact crosslink, paired with fragments from the parent peptide and the entire second peptide ("+P"). Representative alpha-peptide y7/b12 and b4/y15 fragment pairs are highlighted. H_2O_2 oxidation generates an MS-cleavable sulfoxide crosslink, whose HCD produces a dehydrated sulfenic acid fragment on the alpha-peptide ("P[T]") and the corresponding alkene fragment on the beta-peptide ("P[A]"). **F** Butterfly plot comparing annotated spectra for the same peptide and residue pair in the non-oxidized and peroxide-oxidized datasets. Alpha-peptide fragments are purple and beta-peptide fragments are green. Thick lines indicate crosslinker-containing fragments, medium lines indicate standard b/y-ions, and gray lines indicate lossy ions. Key ions from E are highlighted. Source data are provided as a Source Data file. *Created in BioRender. Lab, R. (2026)* https://BioRender.com/t2sjgjj.

crude reaction mixture was passed through Amicon Ultra 3 kDa spin-concentrator and washed with H_2O (5 ×500 μL) to remove the small molecule impurities. The labeled protein was redissolved in 0.1% formic acid in H2O and analyzed using LC–MS.

Synthesis of 4-ONE alkyne

To a solution of furan-2-ylmethanol (2.35 g, 24 mmol, 1 equiv.) in tetrahydrofuran (120 mL) was added sodium hydride (60% w/w in mineral oil, 1.15 g, 28.8 mmol, 1.2 equiv.) portion wise at 0 °C. The resulting suspension was stirred at the same temperature for 10 min, then warmed to room temperature and stirred for an additional 30 min. A solution of propargyl bromide in toluene (80% w/w, 3.5 mL, 36 mmol, 1.5 equiv.) was added portion wise to the reaction mixture upon stirring. The mixture was stirred up to the full conversion of the starting furan-2-ylmethanol. Upon completion, the reaction mixture was cooled to 0 °C, quenched with sat. ammonium chloride (15 ml), diluted with water (50 mL) and extracted with ethyl acetate (3 × 60 mL). The organic phase was washed sequentially with water (50 mL) and brine (50 mL), dried over anhydrous sodium sulfate followed by concentrated in vacuo. The crude reaction mixture was purified through silica gel column chromatography by using 5% hexanes/ethyl acetate as eluent and afforded the desired product 2-((prop-2-yn-1-yloxy) methyl)furan as yellowish liquid.

In a 50 mL round bottom flask containing solution of 12 mL acetone:water (5:1), 2-((prop-2-yn-1-yloxy)methyl)furan (136 mg, 1 mmol, 1 equiv.) and sodium bicarbonate (84 mg, 1 mmol, 1 equiv.) were added sequentially at room temperature. The reaction mixture was then cooled to 0 °C and left to stir for 15 min at the same temperature. In a separate 20 mL scintillation vial, N-bromosuccinimide (178 mg, 1 mmol, 1 equiv.) was dissolved in a solution of 12 mL acetone:water (5:1) and the solution was added to the reaction mixture dropwise. After complete addition of NBS solution, the reaction mixture was left to stir for 10 min at 0 °C. In this time period, the color of the solution changed to yellow. After that, pyridine (80 μL, 2 mmol, 2 equiv.) was added and the reaction mixture was allowed to stir for 2 h at 0 °C. After complete consumption of the starting material (indicated from TLC), the reaction mixture was diluted with ethyl acetate (50 mL) and quenched with 1 N HCl (3 mL). The resulted mixture was extracted with ethyl acetate (3 × 20 mL) and the accumulated organic layer was washed with sat. brine solution (20 mL) and dried over anhydrous sodium sulfate, followed by concentration in vacuo. The crude product was purified through silica gel column chromatography using 20% hexanes/ethyl acetate as eluent to afford 4-ONE Alkyne as a yellowish liquid.

Dose dependent lysate labeling with fluorophore

T-47D cell (Catalog #HTB-133) lysate (100 μg) was treated with various concentrations of 4-ONE and an equimolar amount of propargylamine (for Cys labeling) or alkyne thiol probe (for Lys labeling) in in 200 μL of 9:1 10 mM NaP buffer pH 7.4:ACN at 37 °C and stirred for 12 h. Lysate was precipitated by addition of 1 mL of cold acetone. The protein pellet was centrifuged, dried, and redissolved in pH 7.4 PBS (120 μL) with 20 μL 10% SDS. Click chemistry was performed on each sample through the sequential addition of 20 μL 50 mM copper II sulfate $Cu(SO_4)_2$ in H_2O, 20 μL 60 mM THPTA in H_2O, 20 μL 80 mM ascorbic acid in H_2O, and 2 μL of 10 mM Cy5 azide in DMSO. The reaction was stirred at for 1.5 h, followed by precipitated with 1 mL of cold acetone. The samples were redissolved in Laemmli Sample Buffer with 3% 2-mercaptoethanol and 2% glycerol, heated to 95 °C for 10 min, and loaded on a Novex WedgeWell 4-20% Tris-Glycine gel. The gel was run in Tris-glycine running buffer at 180 V. Next, the gel was analyzed using in-gel fluorescence imaging at 620 nm. The gel was then fixed for 1 h, stained with coomassie brilliant blue for 30 min, and destained overnight.

Dual labeling of lysine in cell lysate with thiol-FITC and Cy5 azide

T-47D cell (Catalog #HTB-133) lysate (100 μg) was dissolved in 175 μL 10 mM NaP buffer pH 7.4 and treated with 20 μL of 4-ONE Alkyne stock in ACN (250 μM final concentration) and 5 μL of 10 mM Thiol FITC fluorophore in DMSO (250 μM final concentration). The reaction was stirred at 37 °C for 12 h. Lysate was precipitated by addition of 1 mL of cold acetone. The lysate pellet was centrifuged, dried, and redissolved in pH 7.4 PBS (120 μL) with 20 μL 10% SDS. Click chemistry was performed with sequential addition of 20 μL 50 mM copper II sulfate $Cu(SO_4)_2$ in H_2O, 20 μL 60 mM THPTA in H_2O, 20 μL 80 mM ascorbic acid in H_2O, and 2 μL of 10 mM Cy5 azide in DMSO. The reaction was stirred for 1.5 h, then lysate was precipitated by addition of 1 mL of cold acetone. The samples were redissolved in Laemmli Sample Buffer with 3% 2-mercaptoethanol and 2% glycerol, heated to 95 °C for 10 min then loaded on a Novex WedgeWell 4–20% Tris-Glycine gel. The gel was run in Tris-glycine running buffer at 180 V. Next, the gel was analyzed using in-gel fluorescence imaging at 470 nm and 620 nm. The gel was then fixed for 1 h, stained with Coomassie Brilliant Blue for 30 min, and destained overnight.

Proteomic analysis of 4-ONE in cell lysate

T-47D cell (Catalog #HTB-133) lysate (100 μg) in 160 μL of 10 mM NaP buffer pH 7.4 was treated with various concentrations of 4-ONE (in 20 μL ACN) and glycine/thioglycolic acid (in 20 μL NaP buffer) and stirred at 37 °C overnight. The modified lysate samples were acetone precipitated using 1 mL cold acetone. The lysate pellet was centrifuged, dried, and then redissolved and digested using SMART Digest™ Trypsin Kit by Thermo Scientific, after which digested peptides were redissolved in 0.1% FA in H_2O and analyzed by LC–MS/MS. This experiment was performed with (n = 2 biological samples).

Fixed cell imaging of 4-ONE alkyne in HeLa cells

HeLa cells (Catalog #CRM-CCL-2) were plated on a plastic cover slip in a 6-well plate at a density of 25,000 cells per well in media and allowed to adhere overnight at 37 °C, 5% CO_2. 4-ONE Alkyne (10 mM stock in

DMSO) was diluted to the final desired concentration of 250 μM in 2 mL of media and incubated with cells for 4 h. The dosage media was removed, and cells were washed with PBS for five min, three times total. A 4% PFA solution in PBS was added to each well and incubated for 10 min. The PFA solution was removed, and cells were washed with PBS for 5 min, three times. A 0.1% Triton X-100 solution was added to each well and incubated for 10 min. The Triton X-100 solution was removed, and cells were washed with PBS for 5 min, three times. A freshly prepared cocktail of 2 mM $Cu(SO_4)_2$, 10 mM THPTA, and 30 mM sodium ascorbate in 10 mL PBS and 20 μL of a 10 mM stock solution of Cy5 azide in DMSO was added to each well. Cells were incubated in this solution for 2 h then washed with PBS for five min, three times total. Cells were mounted onto slides with Fluoroshield with DAPI. Cells were imaged on a Stellaris® 8 Leica DMi8 microscope (20x objective) with fast lifetime contrast (FALCON) module. Samples were excited using a 40 MHz pulsed white light laser tuned to 405 and 633 nm with sequential acquisition. Emitted photons were detected using HyD® S and HyD® X (GaAsP hybrid photocathode). Images were processed and analyzed using ImageJ software. Scale bar = 50 μm.

Enrichment of live-cell 4-ONE crosslinks

All enrichment experiments were performed in biological triplicate (n = 3). For each replicate, 2 mg of T-47D cell (Catalog #HTB-133) lysate dosed with 250 μM 4-ONE alkyne for 4 h during live cell labeling was dissolved in 700 μL pH 7.4 PBS with 40 μL 10% SDS. Click chemistry was performed through the sequential addition of 80 μL 50 mM copper II sulfate $Cu(SO_4)_2$ in H_2O, 80 μL 60 mM THPTA in H_2O, 80 μL 80 mM ascorbic acid in H_2O, and 16 μL of 50 mM Biotin-PEG3-azide in DMSO. Non-specific binding control samples ($n = 3$) were prepared identically, except that the Biotin-PEG3-azide reagent was replaced with an equivalent volume of DMSO, such that no biotin handle was installed on probe-modified proteins. All reactions were stirred at room temperature in the dark for 1.5 h, after which proteins were acetone precipitated by addition of 5 mL of cold acetone. Samples were centrifuged for 10 min at 20,000 × g, the supernatant was removed, and the protein pellet was dried for 15 min. The protein pellet was redissolved in 4 mL of 0.2% SDS in PBS, after which 100 μL of streptavidin agarose beads (washed 3× with PBS) were added. The mixture was rotated overnight at room temperature to perform enrichment, after which the beads were washed with 0.2% SDS in PBS (1 × 10 mL), followed by PBS (3 × 10 mL), and H_2O (3 × 10 mL). The beads were resuspended in 500 μL 6 M urea in PBS, reduced by the addition of neutralized TCEP in 20 μL H_2O stock (10 mM final concentration) for 30 min at r.t., and alkylated by the addition of iodoacetamide in 20 μL H_2O stock (25 mM final concentration) for 30 min at r.t. in the dark. The beads were pelleted by centrifugation for 2 min (1400 × g) and the supernatant was removed. Finally, 10 μg of trypsin dissolved in 300 μL of 2 M urea and 1 mM $CaCl_2$ in 50 mM ammonium bicarbonate buffer was added to the beads. The enriched protein was digested at 37 °C overnight, after which the mixture was acidified to pH 3 using 50 μL 20% FA in H_2O (v/v). The solution was then passed through a C18 peptide desalting column (Thermo Scientific), and the desalted, enriched peptides were redissolved in 0.1% FA in H_2O for LC-MS/MS analysis.

General procedure for pyrrole sulfoxide formation on peptide

Pyrrole peptide (1 mg, 1 equiv.) was dissolved in 887 μL of 1:1 10 mM NaP buffer (pH 7.4):ACN, then 113 μL of 30% (w/v) H_2O_2 was added (final concentration 1 M). The reaction was stirred at room temperature for 2.5 h, after which the reaction was analyzed using (0–80% B over 30 min, solvent B: 0.1% formic acid in MeCN, flow rate: 1 mL/min) and MS to determine the conversion to sulfoxide pyrrole containing peptide.

General procedure for pyrrole sulfoxide formation on single protein

4-ONE-modified/crosslinked protein (1 mg, 1 equiv.) was dissolved in 492 μL of 10 mM NaP buffer (pH 7.4):ACN, then 8.5 μL of 30% (w/v) H_2O_2 was added (final concentration 150 mM). The reaction was stirred at room temperature for 2.5 h, after which the crude reaction mixture was passed through Amicon Ultra 3 kDa spin-concentrator and washed with H_2O (5 ×500 μL) to remove the H_2O_2. The protein was then digested using trypsin and analyzed via HCD–MS/MS to determine crosslinking sites.

Crosslinking of human 26S proteasome

Human 26S proteasome was purified using a biotin-tagged RPN1 (PSMD2) subunit from HCT116 cells[53]. ATP was removed before crosslinking using a 7k MWCO ZebaTM Spin Desalting Column (Thermo Scientific, cat#89882) via centrifugation at 1,000xG at 4 °C with crosslinking buffer (50 mM HEPES (pH 7.5), 100 mM NaCl, and 10% glycerol). RPN1 pulldown was incubated with 4-ONE at 0.5 mM, 1 mM, 2 mM, and 4 mM concentrations from 20x DMSO stocks for 30 min at RT. For non-oxidized samples, protein from all crosslinker concentrations was combined and acetone precipitated at -20 °C for 16 h. For oxidized samples, protein was combined and concentrated using a 3 kDa MWCO column (Amicon, cat#UFC500324), washing twice with 200 μL of crosslinking buffer by centrifugation at 14,000 × g. The protein was then incubated with 150 mM hydrogen peroxide for 2.5 h at RT before washing twice with crosslinking buffer via centrifugation again using a 3 kDa MWCO column and spinning at 16,000xG. The remaining protein was acetone precipitated at −20 °C for 16 h.

Crosslinking mass spectrometry

Crosslink identification was performed by LC-MS/MS[55]. Briefly, acetone-precipitated proteins were pelleted by centrifugation, then subjected to Lys-C endoproteinase digestion for 4 h. Samples were subsequently reduced using dithiothreitol, cysteine residues were alkylated with iodoacetamide, and overnight trypsin digestion was carried out for 16 h. The reaction was quenched by acidification with trifluoroacetic acid to pH 3, and peptides were purified using C18 StageTip desalting[56]. Prior to LC-MS analysis, peptides were separated by size-exclusion chromatography[55]. Dried fractions were reconstituted in 10 μL of 0.1% trifluoroacetic acid/1.6% acetonitrile supplemented with 0.02% n-dodecyl β-D-maltoside, mixed by vortexing, and bath-sonicated for 1 min. Approximately 1 μg of total peptide was loaded onto a Thermo Eclipse Orbitrap mass spectrometer interfaced with a Vanquish Neo UHPLC system. Electrospray ionization was achieved via an EASY-Spray source, and peptide separation was performed on an EASY-Spray PepMap Neo C18 column (75 μm × 500 mm, maintained at 45 °C) preceded by a C18 trap cartridge (5 mm, 5 μm particles, 100 Å pore size; Thermo, cat#03-255-018). Mobile phase A consisted of LC-MS-grade water with 0.1% formic acid; mobile phase B was LC-MS-grade acetonitrile with 0.1% formic acid. Fraction-specific gradient programs (%B) were applied as follows:

Very early SEC fractions: 300 nL/min, 0–1 min (1.6%), 1–10 min (1.6–20.0%), 10–87 min (20.0–38.0%), 87–92.5 min (38.0–55.0%), 92.5–95 min (55.0–76.0%); ramp to 400 nL/min, 95–100 min (76.0%).

Early SEC fractions: 300 nL/min, 0–1 min (1.6%), 1–10 min (1.6–17.6%), 10–87 min (17.6–32.0%), 87–92.5 min (32.0–44.0%), 92.5–95 min (44.0–76.0%); ramp to 400 nL/min, 95–100 min (76.0%).

Early-middle SEC fractions: 300 nL/min, 0–1 min (1.6%), 1–10 min (1.6–16.0%), 10–87 min (16.0–34.0%), 87–92.5 min (34.0–44.0%), 92.5–95 min (44.0–76.0%); ramp to 400 nL/min, 95–100 min (76.0%).

Middle SEC fractions: 300 nL/min, 0–1 min (1.6%), 1–10 min (1.6–10.4%), 10–87 min (10.4–32.8%), 87–92.5 min (32.8–44.0%), 92.5–95 min (44.0–76.0%); ramp to 400 nL/min, 95–100 min (76.0%).

Late SEC fractions: 300 nL/min, 0–1 min (1.6%), 1–10 min (1.6–7.2%), 10–87 min (7.2–25.6%), 87–92.5 min (25.6–44.0%), 92.5–95 min (44.0–76.0%); ramp to 400 nL/min, 95–100 min (76.0%).

Mass spectrometric acquisition used the following global settings: total method duration 85 min, LC infusion mode, expected chromatographic peak width 30 s, advanced peak determination enabled, default charge state 2, EASY-IC internal calibration at run start, NSI source with positive-mode static spray voltage of 2000 V, static gas mode with sweep gas level 2, and ion transfer tube temperature of 280 °C. Survey scans were acquired in the Orbitrap at 240,000 resolution over *m/z* 380–2000 (normal mass range, quadrupole isolation enabled), with an RF lens of 35%, a custom AGC target of 150%, maximum injection time of 100 ms, 1 microscan, profile mode, positive polarity, and 10 V source fragmentation. Data-dependent triggering required MIPS peptide classification, a minimum precursor intensity of 2.5×10^4, precursor charge states 3–7, and dynamic exclusion after one occurrence within a 10 s window (±10 ppm mass tolerance) with isotope exclusion and single-charge-state dependent scanning both active. A 3 s duty cycle was employed.

Fragmentation was managed through two acquisition priority branches. Priority 1 targeted higher charge states via three subbranches: (A) charge state 5, m/z 380–1800; (B) charge states 6–7, m/z 380–1350; (C) charge state 4, *m/z* 380–1000. Following intensity-ranked precursor sorting, HCD MS2 spectra were collected in the Orbitrap at 60,000 resolution (m/z 150–2000) using quadrupole isolation (1.4 m/z window), stepped normalized collision energies of 18, 26, and 30%, an AGC target of 750%, maximum injection time of 250 ms, 1 microscan, and centroid mode. Priority 2 targeted charge state 3 precursors across m/z 380–2000 with otherwise identical MS2 acquisition parameters (quadrupole isolation, 1.4 m/z window; stepped HCD at 18, 26, 30%; Orbitrap detection at 60,000 resolution; AGC 750%; maximum injection time 250 ms; centroid mode).

Raw data files were processed into recalibrated mgf files[55]. xiSEARCH(v.1.8.6)[57] was utilized to search the recalibrated mgf files against a protein FASTA database containing 53 protein sequences (proteins found with a relative abundance >5E8 with at least three unique peptides in a linear digest injected in triplicate). The following xiSEARCH configuration was used for the search for the non-oxidized samples: carbamidomethyl (C, 57.021464, variable), deamidation (N, 115.026397 (delta mass), variable), oxidation (M, 147.035395 (delta mass), variable), pyroglutamate (N-terminal Q, -17.026549105, variable), 4-ONE-Schiff base formation (K, 136.05242, variable), dihydroxyl (W/M, 31.989829, variable), kynurenine formation (W, 3.994915, variable), 4-ONE-Unreacted (K, 154.09938, linear), water loss (S/T/D/E/C-terminal, 18.01056027), ammonia loss (R/K/N/Q/N-terminal, 17.02654493), methionine hydroxylation loss (M, 63.99828547), trypsin digest, 3 missed cleavages allowed, 4-ONE crosslink (K/N-terminal to C, 118.07825), non-covalent crosslink, MS1 tolerance of 2.0 ppm, MS2 tolerance of 5.0 ppm, and 3 max modifications per peptide.

The above configuration was used to search the peroxide-oxidized crosslinking data with the following changes: cysteic acid (C, 47.9852, variable), cleavable crosslinker fragment "A" (-33.98772), cleavable crosslinker fragment "T" (150.0503153), 4-ONE crosslink (K/N-terminal to C, 134.07316).

The resulting xiSEARCH csv outputs were manually filtered to require at least one "unique crosslinked matched conservative" and three "total fragment matches" for both peptides 1 and 2. These filtered outputs were then used to calculate a 5% residue-pair false-discovery rate using xiFDR (v.2.2.1, https://www.rappsilberlab.org/software/xifdr/)[58]. xiFDR outputs were uploaded to xiVIEW[59] (www.xiview.org) to generate both spectra and ChimeraX pseudobonds for a structure of the 26S proteasome (PDB ID: 6MSE)[51].

Reporting summary

Further information on research design is available in the Nature Portfolio Reporting Summary linked to this article.

Data availability

All data supporting the findings of this study are available within the supplementary information. These include the synthesis of the probes, optimization of the reaction conditions, the procedure of modification on peptides, intact proteins, cell lysates, chemoselectivity studies, cytotoxicity studies, cellular imaging, chemoproteomic profiling, and product characterization by NMR, HPLC, LC–MS, MS/MS, and HRMS. The mass spectrometry proteomics data generated in this study have been deposited to the ProteomeXchange Consortium via the PRIDE partner repository[60] with the dataset identifiers PXD070252, PXD077820, and PXD077887. Protein identification was performed with the human Swiss-Prot database (20,456 entries). Supplementary data are provided with this paper. Source data are provided with this paper.

References

1. Lorand, L. & Graham, R. M. Transglutaminases: crosslinking enzymes with pleiotropic functions. *Nat. Rev. Mol. Cell Biol.* **4**, 140–156 (2003).
2. Griffin, M., Casadio, R. & Bergamini, C. M. Transglutaminases: nature's biological glues. *Biochem. J.* **368**, 377–396 (2002).
3. Paikin, Z. E. et al. Acrolein-mediated conversion of lysine to electrophilic heterocycles for protein diversification and toxicity profiling. *J. Am. Chem. Soc.* **147**, 5679–5692 (2025).
4. Esterbauer, H., Schaur, R. J. & Zollner, H. Chemistry and biochemistry of 4-hydroxynonenal, malonaldehyde and related aldehydes. *Free Radic. Biol. Med.* **11**, 81–128 (1991).
5. Uchida, K. 4-Hydroxy-2-nonenal: a product and mediator of oxidative stress. *Prog. Lipid Res.* **42**, 318–343 (2003).
6. Paikin, Z. E., Villalobos Galindo, A. & Raj, M. Metabolite-mediated protein macrocyclization. *Synlett* **36**, 1379–1384 (2025).
7. Doorn, J. A. & Petersen, D. R. Covalent adduction of nucleophilic amino acids by 4-hydroxynonenal and 4-oxononenal. *Chem. Biol. Interact.* **143–144**, 93–100 (2003).
8. Keller, J. N. et al. 4-Hydroxynonenal, an aldehydic product of membrane lipid peroxidation, impairs glutamate transport and mitochondrial function in synaptosomes. *Neuroscience* **80**, 685–696 (1997).
9. Perluigi, M., Coccia, R. & Butterfield, D. A. 4-Hydroxy-2-nonenal, a reactive product of lipid peroxidation, and neurodegenerative diseases: a toxic combination illuminated by redox proteomics studies. *Antioxid. Redox Signal.* **17**, 1590–1609 (2012).
10. Wong, C. M. et al. Protein carbonylation as a novel mechanism in redox signaling. *Circ. Res.* **102**, 310–318 (2008).
11. Villalobos Galindo, A. & Raj, M. Solvent-dependent chemoselectivity switch to Arg–Lys imidazole cross-links. *Org. Lett.* **26**, 8356–8360 (2024).
12. Guo, P. et al. Peptide stapling by crosslinking two amines with α-ketoaldehydes through diverse modified glyoxal-lysine dimer linkers. *Angew. Chem. Int. Ed. Engl.* **63**, e202318893 (2024).
13. Villalobos Galindo, A. et al. Cooperative aldehyde chemistry maps an orthogonal lysine reactivity landscape. *J. Am. Chem. Soc.* **148**, 15125–15137 (2026).
14. Talbott, J. M. et al. Spatiotemporal imaging of catechol aldehydes in neural tissue. *JACS Au* **5**, 1717–1727 (2025).
15. Welling, M. et al. Rapid biopolymerisation during wound plug formation in green algae. *J. Adhes.* **85**, 825–838 (2009).
16. Weissflog, J., Adolph, S., Wiesemeier, T. & Pohnert, G. Reduction of herbivory through wound-activated protein cross-linking by the invasive macroalga Caulerpa taxifolia. *ChemBioChem* **9**, 29–32 (2008).

17. Sinz, A. Chemical cross-linking and mass spectrometry to map three-dimensional protein structures and protein–protein interactions. *Mass Spectrom. Rev.* **25**, 663–682 (2006).
18. Chavez, J. D. & Bruce, J. E. Chemical cross-linking with mass spectrometry: a tool for systems structural biology. *Curr. Opin. Chem. Biol.* **48**, 8–18 (2019).
19. Hossain, M. A. et al. Evaluating protein cross-linking as a therapeutic strategy to stabilize SOD1 variants in a mouse model of familial ALS. *PLoS Biol.* **22**, e3002462 (2024).
20. Müller, F. et al. Developing a new cleavable crosslinker reagent for in-cell crosslinking. *Commun. Chem.* **8**, 191 (2025).
21. Gutierrez, C. B. et al. Development of a novel sulfoxide-containing MS-cleavable homobifunctional cysteine-reactive cross-linker for studying protein–protein interactions. *Anal. Chem.* **90**, 7600–7607 (2018).
22. Zhang, Y. et al. Novel urazole-derived MS-cleavable cross-linkers targeting tyrosine/lysine residues for protein structural analysis. *Anal. Chem.* **97**, 15190–15198 (2025).
23. Yu, C. et al. Trioxane-based MS-cleavable cross-linking mass spectrometry for profiling multimeric interactions of cellular networks. *Nat. Commun.* **16**, 5585 (2025).
24. Liu, F. & Heck, A. J. R. Interrogating the architecture of protein assemblies and protein interaction networks by cross-linking mass spectrometry. *Curr. Opin. Struct. Biol.* **35**, 100–108 (2015).
25. Lin, D. et al. 4-Oxo-2-nonenal is both more neurotoxic and more protein reactive than 4-hydroxy-2-nonenal. *Chem. Res. Toxicol.* **18**, 1219–1231 (2005).
26. Ishii, T. et al. Characterization of acrolein-induced protein cross-links. *Free Radic. Res.* **41**, 1253–1260 (2007).
27. Uchida, K., Hasui, Y. & Osawa, T. Covalent attachment of 4-hydroxy-2-nonenal to erythrocyte proteins. *J. Biochem.* **122**, 1246–1251 (1997).
28. Sun, R. et al. Chemoproteomics reveals chemical diversity and dynamics of 4-oxo-2-nonenal modifications in cells. *Mol. Cell. Proteom.* **16**, 1789–1800 (2017).
29. Zhu, X. et al. Mass spectrometric characterization of protein modification by the products of nonenzymatic oxidation of linoleic acid. *Chem. Res. Toxicol.* **22**, 1386–1397 (2009).
30. Börgel, J. & Ritter, T. Late-stage functionalization. *Chem* **6**, 1877–1887 (2020).
31. deGruyter, J. N., Malins, L. R. & Baran, P. S. Residue-specific peptide modification: a chemist's guide. *Biochemistry* **56**, 3863–3873 (2017).
32. Lin, S. et al. Redox-based reagents for chemoselective methionine bioconjugation. *Science* **355**, 597–602 (2017).
33. Wang, W., Lorion, M. M., Shah, J., Kapdi, A. R. & Ackermann, L. Late-stage peptide diversification by position-selective C–H activation. *Angew. Chem. Int. Ed. Engl.* **57**, 14700–14717 (2018).
34. Wang, Y., Czabala, P. & Raj, M. Bioinspired one-pot furan-thiol-amine multicomponent reaction for making heterocycles and its applications. *Nat. Commun.* **14**, 4086 (2023).
35. He, S. et al. Separation and nanoencapsulation of antitumor peptides from Chinese three-striped box turtle (*Cuora trifasciata*). *J. Microencapsul.* **33**, 344–354 (2016).
36. Herradura, P. S., Pendola, K. A. & Guy, R. K. Copper-mediated cross-coupling of aryl boronic acids and alkyl thiols. *Org. Lett.* **2**, 2019–2022 (2000).
37. Parker, C. G. & Pratt, M. R. Click chemistry in proteomic investigations. *Cell* **180**, 605–632 (2020).
38. Speers, A. E. & Cravatt, B. F. Profiling enzyme activities in vivo using click chemistry methods. *Chem. Biol.* **11**, 535–546 (2004).
39. Speers, A. E., Adam, G. C. & Cravatt, B. F. Activity-based protein profiling in vivo using a copper(I)-catalyzed azide–alkyne [3+2] cycloaddition. *J. Am. Chem. Soc.* **125**, 4686–4687 (2003).
40. Cravatt, B. F., Wright, A. T. & Kozarich, J. W. Activity-based protein profiling: from enzyme chemistry to proteomic chemistry. *Annu. Rev. Biochem.* **77**, 383–414 (2008).
41. Speers, A. E. & Cravatt, B. F. A tandem orthogonal proteolysis strategy for high-content chemical proteomics. *J. Am. Chem. Soc.* **127**, 10018–10019 (2005).
42. O'Shea, J. P. et al. pLogo: a probabilistic approach to visualizing sequence motifs. *Nat. Methods* **10**, 1211–1212 (2013).
43. Zhou, Y. et al. Metascape provides a biologist-oriented resource for the analysis of systems-level datasets. *Nat. Commun.* **10**, 1523 (2019).
44. Ge, S. X., Jung, D. & Yao, R. ShinyGO: a graphical gene-set enrichment tool for animals and plants. *Bioinformatics* **36**, 2628–2629 (2020).
45. Butterfield, D. A. & Halliwell, B. Oxidative stress, dysfunctional glucose metabolism and Alzheimer disease. *Nat. Rev. Neurosci.* **20**, 148–160 (2019).
46. Kolbowski, L. et al. Improved peptide backbone fragmentation is the primary advantage of MS-cleavable crosslinkers. *Anal. Chem.* **94**, 7779–7786 (2022).
47. Kao, A. et al. Development of a novel cross-linking strategy for fast and accurate identification of cross-linked peptides of protein complexes. *Mol. Cell. Proteom.* **10**, M110.002212 (2011).
48. Hagen, S. E. et al. Synthesis of CID-cleavable protein crosslinking agents containing quaternary amines for structural mass spectrometry. *Org. Biomol. Chem.* **16**, 6867–6870 (2018).
49. Jiao, F. et al. Cysteine-enabled cleavability to advance cross-linking mass spectrometry for global analysis of endogenous protein-protein interactions. *Nat. Commun.* **16**, 11093 (2025).
50. Sjöberg, B. et al. Methionine oxidation by hydrogen peroxide in peptides and proteins: a theoretical and Raman spectroscopy study. *J. Photochem. Photobiol. B* **188**, 95–99 (2018).
51. Dong, Y. et al. Cryo-EM structures and dynamics of substrate-engaged human 26S proteasome. *Nature* **565**, 49–55 (2019).
52. Finley, D., Chen, X. & Walters, K. J. Gates, channels, and switches: elements of the proteasome machine. *Trends Biochem. Sci.* **41**, 77–93 (2016).
53. Negi, H. et al. An engineered cell line with a hRpn1-attached handle to isolate proteasomes. *J. Biol. Chem.* **299**, 104948 (2023).
54. Chen, X. et al. Proteasome interaction with ubiquitinated substrates: from mechanisms to therapies. *FEBS J.* **288**, 5231–5251 (2021).
55. Ciancone, A. et al. Expanding the crosslinking mass spectrometry toolbox with vinyl sulfone crosslinkers. *Mol. Cell. Proteom.* **24**, 101315 (2025).
56. Rappsilber, J., Mann, M. & Ishihama, Y. Protocol for micro-purification, enrichment, pre-fractionation and storage of peptides for proteomics using StageTips. *Nat. Protoc.* **2**, 1896–1906 (2007).
57. Mendes, M. L., Fischer, L. & Chen, Z. A. An integrated workflow for crosslinking mass spectrometry. *Mol. Syst. Biol.* **15**, e8994 (2019).
58. Lenz, S. et al. Reliable identification of protein-protein interactions by crosslinking mass spectrometry. *Nat. Commun.* **12**, 3564 (2021).
59. Combe, C. W., Graham, M. & Kolbowski, L. xiVIEW: visualization of crosslinking mass spectrometry data. *J. Mol. Biol.* **436**, 168656 (2024).
60. Perez-Riverol, Y. et al. The PRIDE database at 20 years: 2025 update. *Nucleic Acids Res.* **53**, D543–D553 (2025).

Acknowledgements

We gratefully acknowledge the Systems Mass Spectrometry Core at the Institute of Bioengineering and Bioscience, Georgia Institute of Technology, for their exceptional support. The proteomics data were acquired on an Exploris 480 or timsTOF HT funded by NIH S-10 grant number 1S10OD038327-01. Special thanks to Ludyanna Lebon and Dr Rakesh Singh for their invaluable expertise and support in running the

samples and analysis of the proteomics data. This work was supported by the Emory University Integrated Cellular Imaging Core Facility (RRID: SCR_023534) and Winship Flow Cytometry Core (RRID: SCR_022324). This study was supported in part by the Emory Glycomics and Molecular Interactions Core (EGMIC; RRID: SCR_023524), with additional support provided by the National Center for Advancing Translational Sciences of the National Institutes of Health under Award Number UL1TR002378. J.M. Talbott acknowledges the ARCS Foundation for support. The contributions of the NIH authors were made as part of their official duties as NIH federal employees, are in compliance with agency policy requirements, and are considered Works of the United States Government; however, the findings and conclusions presented in this paper are those of the authors and do not necessarily reflect the views of the NIH or the U.S. Department of Health and Human Services. We thank Dr Kitaik Lee for mapping the crosslinks, both non- and H_2O_2-oxidized, against different proteasome structures. The content is solely the responsibility of the authors and does not necessarily reflect the official views of the National Institutes of Health. All graphs were produced in Prism, and all figures were created with BioRender.com and Adobe Illustrator.

Author contributions

Z.E.P. and M.R. conceived the project. Z.E.P. synthesized 4-ONE, performed initial peptide modification and chemoselectivity studies, peptide stapling and macrocyclization, and solid-support modification. S.K. synthesized 4-ONE alkyne and generated the cytotoxic peptide library. S.M. separated the regioisomers and carried out full characterization of the pyrrole products. Z.E.P. conducted all protein studies and gel electrophoresis. J.M.T. conducted cellular imaging and flow cytometry studies. Z.E.P. developed COSMIc and carried out proteome profiling experiments. H.N. and K.J.W. isolated 26S proteasome. A.M.C. and F.J.O. performed 4-ONE proteasome crosslinking studies. Z.E.P. and B.Q.G.L. analyzed chemoproteomic data. Z.E.P., J.M.T., A.M.C., F.J.O., and M.R. wrote the manuscript. All authors edited the final manuscript.

Funding

M. Raj discloses support for the research of this work from the National Institutes of Health [1R01HG012941-01] and the National Science Foundation [CHE-2406996]. K.J. Walters discloses support for the research of this work from the Intramural Research Program of the National Institutes of Health, National Cancer Institute, Center for Cancer Research [1 ZIA BC011490, 1 ZIA BC011627]. F.J. O'Reilly discloses support for the research of this work from the Intramural Research Program of the National Institutes of Health, National Cancer Institute, Center for Cancer Research [ZIA BC012114-03], the Frederick National Laboratory for Cancer Research, National Institutes of Health [HHSN261200800001E], and the American Lebanese Syrian Associated Charities (ALSAC).

Competing interests

The authors declare no competing interests.

Additional information

Supplementary information The online version contains supplementary material available at https://doi.org/10.1038/s41467-026-74843-x.

Correspondence and requests for materials should be addressed to Monika Raj.

Peer review information *Nature Communications* thanks anonymous reviewers for their contribution to the peer review of this work. A peer review file is available.